Sloss, Craig R., Nothdurft, Luke, Hua, Quan, O'Connor, Shoshannah G., Moss, Patrick T., Rosendahl, Daniel, Petherick, Lynda M., Nanson, Rachel A., Mackenzie, Lydia L., Sternes, Alison, Jacobsen, Geraldine E., and Ulm, Sean (2018) *Holocene sea-level change and coastal landscape evolution in the southern Gulf of Carpentaria, Australia.* Holocene, 28 (9) pp. 1411-1430.

https://doi.org/10.1177/0959683618777070

Holocene sea-level change and coastal landscape evolution in the southern Gulf of Carpentaria, Australia: A review

Craig R. Sloss[a,*], Luke Nothdurft[a], Quan Hua[b], Shoshannah G. O'Connor[a], Patrick T. Moss[c], Daniel Rosendahl[d], Lynda M. Petherick[e], Rachel A. Nanson[f], Lydia L. Mackenzie[c], Sternes, A[a]., Geraldine E. Jacobsen[b], Sean Ulm[d,g]

[a] School of Earth, Environmental and Biological Sciences, Queensland University of Technology, GPO Box 2434, Brisbane, QLD, 4001, Australia

[b] Australian Nuclear Science and Technology Organisation, Locked Bag 2001, Kirrawee DC, NSW 2232, Australia

[c] School of Earth and Environmental Sciences, The University of Queensland, Brisbane, QLD, 4072, Australia

[d] College of Arts, Society and Education, James Cook University, PO Box 6811, Cairns, QLD 4870, Australia

[e] School of Geography, Environment and Earth Sciences, Victoria University of Wellington, PO Box 600, Wellington, New Zealand

[f] Geoscience Australia, Canberra.

[g] ARC Centre of Excellence for Australian Biodiversity and Heritage, James Cook University, PO Box 6811, Cairns, QLD 4870, Australia

* Corresponding author

Abstract

A revised Holocene sea-level history for the southern Gulf of Carpentaria is presented based on new data from the South Wellesley Archipelago and age recalibration of previous research. Results confirm that rising sea levels during the most recent post-glacial marine transgression breached the Arafura Sill ca. 11,700 cal. yr BP. Sea levels continued to rise to ca. -30 m by 10,000 cal. yr BP, leading to full marine conditions. By 7,700 cal. yr BP sea-level reached present mean sea-level (PMSL) and continued to rise to an elevation of between 1.5 m and 2 m above PMSL. Sea-level remained ca. +1.5 between 7,000 – 4,000 cal. yr BP, followed by rapid regression to within ±0.5 m of PMSL by ca. 3,500 cal. yr BP. Earlier research suggested that the mid-Holocene highstand was due to hydrostatic loading in the central basin of the Gulf of Carpentaria. Results from this study indicate that eustatic sea-level change is the dominate influence on sea-level fluctuations, rather than hydro-isostatic adjustment. Results from this research also highlight the difference between the prolonged highstand observed along the eastern sea-board of Australia versus the short highstand observed in the Gulf of Carpentaria and other far-field sites. The driving force behind the difference is hypothesized here to be a greater influence of equatorial ocean siphoning from the lower latitudes and a prolonged melt-water input from Antarctica. The combined effects explain the short highstand in the tropical north of Australia and the extended highstand in higher latitudes around the Australian continental margin.

Keywords: Australasia; eustatic; far-field; geomorphology, coastal; Holocene; sea-level change

1. Introduction

The study of Holocene sea-level histories and coastal landscape response is fundamental to our understanding of how coastal environments will respond to future sea-level and climate change. It is also essential to understand the drivers of these sea-level and coastal landscape changes to better adapt to coastal environmental change. The Gulf of Carpentaria is an ideal locality for investigating changes in sea-level over the last glacial cycle. Positioned in a relatively tectonically stable portion of the Indo-Australian Plate, the southern Gulf of Carpentaria is positioned in a far field region unaffected by glacio-isostasy. Located between Australia and New Guinea, the Gulf of Carpentaria is an epicontinental sea extending from 10ºS to 18ºS, and covering an area of around 230,000 km^2 (Fig. 1A). At present, the Gulf of Carpentaria is connected to the Coral Sea in the northeast by the Torres Strait with water depths of up to 12 m. To the northwest, the Gulf is connected to the Arafura Sea through the Arafura Sill, with water depths of up to 53 m (Fig. 1A; Chivas et al., 2001; Reeves et al., 2008). The seafloor in the Gulf is a relatively flat, featureless plain between 50 and 60 m water depth, with the greatest water depth of 70 m in the central eastern basin (Torgersen et al., 1983, 1988). The shallowness of the receiving basin, and restriction from marine influences during lowstands in sea-level provide an ideal location to investigate major phases of marine transgression and regression, recording fully marine, estuarine and lacustrine depositional environments for the past 200,000 years (Torgersen et al., 1983, 1988; Chivas et al., 2001; Reeves et al., 2007, 2008, 2013).

Previous research into sea-level change following the Last Glacial Maximum (LGM) indicated that rising sea levels during the most recent post-glacial marine transgression (PMT) breached the restricting Arafura sill between 12,000 and 11,500 cal. yr BP and that the culmination of PMT occurred between 6,500–6,000 cal. yr BP, reaching a maximum of 2 m above present mean sea-level (PMSL) in the southern region of the Gulf of Carpentaria (Rhodes et al. 1980; Chappell et al. 1982). The Holocene highstand was short-lived, and sea-level fell smoothly to present level over the last 6,000 years. Rhodes et al. (1980) and Chappell et al. (1982) attribute the relative sea-level fall to hydro-isostatic loading in the northern and central basin, and on the eastern Australian continental shelf. The hydro-isostatic loading resulting in differential crustal movement across north Queensland, represented by regional subsidence in the northeast and uplift of between 0.2 – 1.4 m for the western Cape (Edward River), and 1.7 – 3.1 m in the Flinders-Leichhardt Region (Karumba; Fig. 1A; Chappell et al. 1982).

This study presents a revised Holocene sea-level history based on a review of previous research from the southern Gulf of Carpentaria and additional data collected from elevated coral reefs, beach-rock and aeolianite deposits, cores from beach ridges, mudflats and mangrove swamps, survey of wave-cut erosional features, and dating of *in situ* encrusting organisms. Results provide a more detailed Holocene sea-level reconstruction and show a similar mid-Holocene sea-level history to those identified on the east coast of Australia (Sloss et al., 2005, 2007; Woodroffe et al., 2007; Lewis et al., 2013). The consistency between sea-level histories from eastern Australia and the Gulf of Carpentaria suggest that higher sea-levels following the most recent PMT and the mid-to-late Holocene regression occur over a larger regional scale than previously recognized. Results indicate that Holocene sea-level histories are driven by regional eustatic driving forces, and not by localized hydro-isostatic influences.

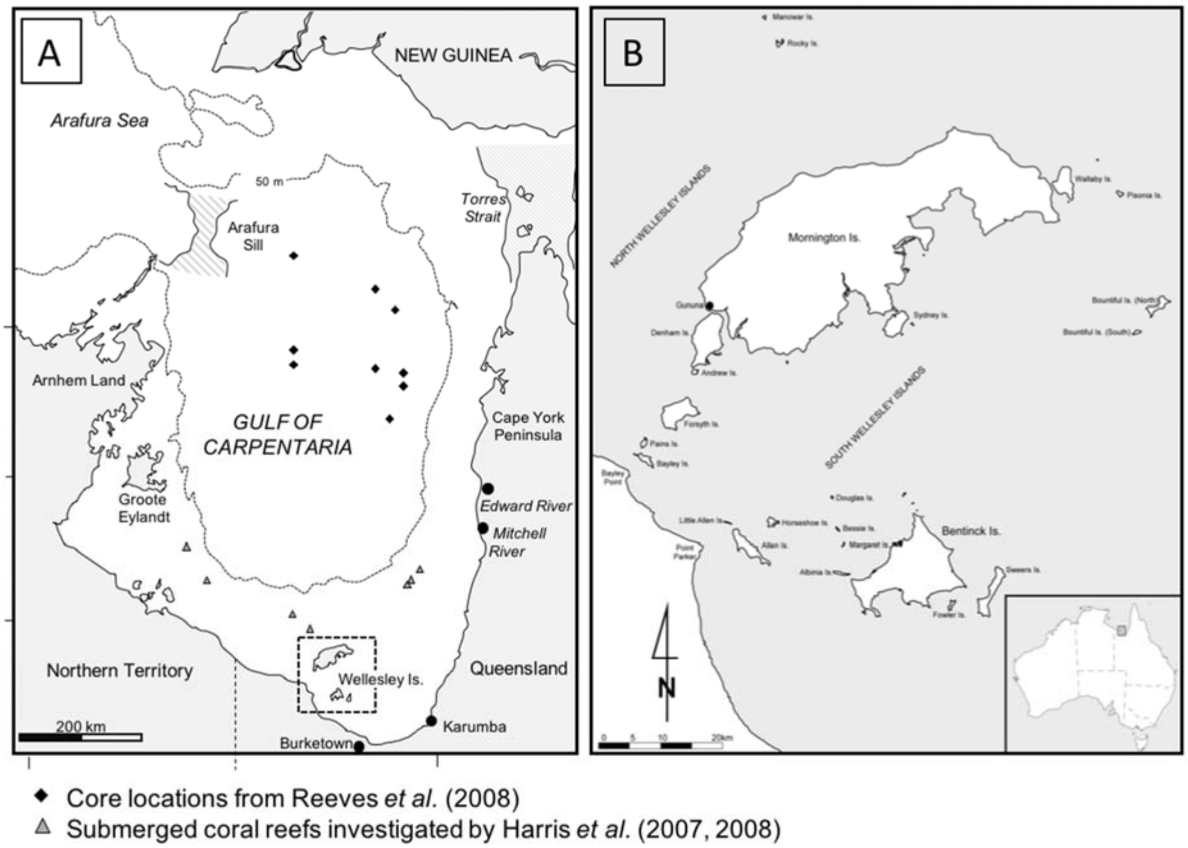

Figure 1: Location of (A) the Gulf of Carpentaria, northern Australia; (B) Wellesley Island including the study sites, Bentinck, Sweers, Albinia and Fowler Islands.

2. Study Site: Wellesley Archipelago and adjacent mainland coast

The Wellesley Archipelago is a group of 23 islands in the southern Gulf of Carpentaria. Mornington (the northernmost and largest island at ca. 950 km^2) and Bentinck Island (ca. 150 km^2) comprise the traditional country of Lardil and Kaiadilt people respectively. The remainder of the archipelago comprises smaller islands including Sweers, Fowler, Albinia, Horseshoe, Forsyth and Allen Islands (Figs 1B). Yangkaal people own the islands between Mornington and the mainland, while the islands closest to the mainland have shared ownership between Yangkaal, Kaiadilt and the mainland Gangalidda people (Memmott et al., 2016).

Located between the latitudes of 16°17’S and 17°09’S and longitudes of 139°02’E and 139°54’E, the Wellesley islands have a tropical climate with a hot, wet summer monsoonal season and a warm, dry winter season. Summer air temperatures range from 28 – 35°C and winter air temperatures range from 22 – 30°C. Ninety-two percent of the average 1200 mm rainfall occurs from November to March, associated with the Australian Monsoon and cyclones (Bureau of Meteorology, 2016). Within the southern Gulf of Carpentaria, the Neap tidal range averages 3 m, and reaches up to 4 m during spring tides (Church and Forbes, 1981; Rhodes et al., 1980; Wolanski, 1993).

The core of the islands is composed of Jurassic to Early Cretaceous fluvial and marine sedimentary successions comprising alternating sandstones, clayey sandstones and siltstones (the Normanton Formation) (Grimes 1979; Smart et al. 1980; Day 1983). The Normanton Formation is heavily weathered to a sandy lateritic surface with little relief, often forming wave-cut cliffs and platforms in coastal outcrop. The islands presently preserve a diverse range of Holocene coastal environments, including beach ridge systems, mangrove fringe and intertidal mud- and sandflats, and significant exposures of aeolianite. The adjacent coastal mainland sites include broad chenier plains and beach ridge deposits, first described by Rhodes et al. (1980) and Rhodes (1982). At some locations, shore parallel chenier ridge systems have prograded over 30 km since the mid-Holocene between Karumba and Burketown (Rhodes, 1982; Fig. 1A).

3. Background

Over the late Quaternary the Gulf has been repeatedly submerged and exposed by fluctuating sea-levels with depositional environments shifting between open ocean to estuarine, lacustrine and subaerial exposure (Chivas et al., 2001; Reeves et al., 2008). Using micro-palaeontological indicators and radiocarbon age determinations Yokoyama et al. (2000, 2001a, 2001b) identified that sea-level was 120 m below PMSL during the LGM. During this time the Arafura and Torres Strait sills isolated the Gulf of Carpentaria from marine inundation, resulting in an extensive basin occupied by a large lake (Lake Carpentaria) up to 250 km in width, 500 km in length, and approximately 15 m deep (Jones and Torgersen, 1988; Torgersen et al., 1988; Yokoyama et al., 2001a, 2001b; Reeves et al., 2008).

Detailed palaeoecological and sedimentary analysis of lacustrine and marine basin sediments by Chivas et al. (2001) and Reeves et al. (2008) indicate that rising sea-levels during the most recent post-glacial marine transgression breached the Arafura Sill ca. 12,000 cal. yr BP, with full marine conditions being attained by 10,500 cal. yr BP. U-series dating of drowned coral reefs in the southern Gulf of Carpentaria indicate that reef growth commenced between 10,500 and 9,500 cal. yr BP and continued to flourish until ca. 7,000 cal. yr BP (Harris et al., 2007, 2008; Fig. 1A).

The principal records for the timing and elevation of the culmination of most recent PMT sea-levels in the southern Gulf of Carpentaria derive from chenier ridges and beach ridge systems at Karumba and Edward River (Chappell et al., 1982; Rhodes et al., 1980; Rhodes, 1982; Fig. 1). Previous research utilising radiocarbon age determinations on *Tegillarca granosa* (syn. *Anadara granosa*) sampled from chenier and beach ridge deposits suggested that sea-level was higher (ca. +2.2 m) ca. 6,000 – 5,500 cal. yr BP, before falling smoothly to its present level (original ^{14}C ages in Rhodes et al., 1980; Chappell et al., 1982; Rhodes, 1982, calibrated for this study, see Table 3). This record of higher sea-level in the mid-Holocene provided one of the key datasets for modelling of hydro-isostatic adjustment in northern Queensland (Chappell et al., 1982, 1983).

3.1 Sea-level Proxies

To determine the indicative meaning of a sea-level "index point" it is critical to establish the accuracy and precision of the elevation of the index point in relation to PMSL (Shennan and Horton, 2002; Engelhart et al., 2009; Rovere et al., 2016). In this section we review the various sea-level index points used in previous research and in this study. Proxies include chenier and beach ridge systems, aeolianite deposits, *in situ* oyster beds and bioherms, intertidal and subtidal sedimentary successions, and erosional features. A critical assessment of the indicative meaning of the various proxies in relation to their contemporary sea-level at the time of deposition and/or formation, stratigraphic context, post-deposition alteration, and their position relative to PMSL (Australian Height Datum, equivalent to PMSL) are assessed (Woodroffe and Chappell, 1993; Sloss et al., 2007; Lewis et al., 2013). This incorporates establishing the indicative range (IR; the vertical range associated with the index point) and the reference water level (RWL; mid-point of the IR) in relation to PMSL (Shennan and Horton, 2002; Engelhart et al., 2009; Rovere et al., 2016). The indicative meaning is established using the formulas modified after Rovere et al. (2016):

Eq. 1: $RWL = \frac{U1+L1}{2}$

Eq. 2: $IM = E - RWL$

Eq. 3: $IM_e = \sqrt{E_e^2 + (\frac{IR}{2})^2}$

Where:

$U1$ = Upper limit of modern analogue.

$L1$ = Lower limit of modern analogue.

RWL = Mid-point of modern analogue (PMSL).

IR = Indicative range of sea-level index point.

E = Elevation of sea-level index point.

E_e = Elevation error associated with field measurement of index point.

IM = Indicative meaning of sea-level index point.

IM_e = Vertical error associated with the indicative meaning of sea-level index point.

The modern analogue range in this study is taken from the maximum spring tide range (4 m) or in some specific cases the maximum neap tide range (3 m) observed in the Gulf of Carpentaria. The indicative meaning (*IM*) of the index points are expressed as elevations relative to PMSL (AHD), as opposed to sample elevation above AHD.

3.1.1 Chenier ridge systems

Chenier ridges are wave-built landforms, deposited within the high-tide to supra-tidal zone and comprising two or more parallel to sub-parallel stranded ridges (cheniers) of coarse sediment (sand, gravel or shell). Such features are common on open coasts with low-to-moderate wave-energy environments with the coarse chenier ridges over finer-grained intertidal deposits (Otvos and Price, 1979; Augustinus et al., 1989; Otvos, 2004, 2005; McBride et al., 2007; Weill et al., 2012). Formation occurs with the onshore migration of coarse sediment with rising tides and wave bores to the High-Water Spring Tide (HWST) and mean High-Water Neap Tide (HWNT) (McBride et al., 2007; Weill et al., 2012). As the ridge crest grows above the mean HWST they become less frequently submerged and are starved of sediment (Weill et al., 2012). A chenier plain forms when two or more sets of chenier ridges are separated by fine-grained intertidal deposits and are characteristic of prograding coastlines (Otvos, 2004, 2005; McBride et al., 2007). The formation of chenier ridges and plains is also strongly influenced by episodic sediment supply (seasonal), as well as the influence of storms, sea-level fluctuations, longshore currents, tidal dynamics and delta development (Augustinus, 1989; Saito et al., 200l; Nott, 1996; McBride et al., 2007; Dougherty and Dickson, 2012).

Despite the dynamic depositional processes, the transition between the chenier ridges and underlying intertidal muds can be used to reconstruct Holocene sea-level histories (e.g. Rhodes et al., 1980; Rhodes, 1982; Wang and Van Strydonck, 1997; Saito et al., 2000; McBride et al., 2007; Dougherty and Dickson, 2012; Weill et al., 2012). Dougherty and Dickson (2012) demonstrated that a clear stratigraphic boundary exists between chenier ridges and underlying intertidal mud facies using Ground Penetrating Radar (GPR) across the Miranda chenier plain on the North Island of New Zealand. Dougherty and Dickson (2012) identified the upper limit of this stratigraphic transition to be the equivalent of the HWST, and concluded changes in sea-level controlled chenier spacing. Their research showed that a sea-level highstand of approximately +2 m above PMSL occurred ca. 4,000 years ago and fell to present levels ca. 1,000 years ago (Dougherty and Dickson, 2012).

Accordingly, chenier ridges provide a proxy for palaeo-sea-level (between HWNT to HWST), but cannot provide an upper limit, as they can be deposited above mean sea-level (Fig. 2). Age determination from chenier ridges must also be used with caution as faunal components are transported and reworked, and any age determinations require careful assessment of the accuracy, precision and relevance of the chronological framework developed. In this study, an indicative meaning for chenier ridge as a sea-level proxy is taken from the facies transition from intertidal and subtidal mudflat deposits with the overlying chenier ridge representing an indicative range (*IR*) of 1.5 to 2 m above PMSL and an indicative meaning (*IM*) of +1.75 m (Fig. 2).

3.1.2 Beach ridge systems

Beach ridge deposits are parallel to sub-parallel elongate mounds of fine-grained sand to boulder size material, comprising of siliciclastic or bio-clastic sediments. Beach ridges form from the interplay of nearshore processes (tides, currents and waves), sediment supply and physical characteristics (e.g. grain size and lithology), and are common features on prograding coasts with a minimum amount of accommodation space, flat nearshore topography, and abundant sediment supply (Taylor and Stone, 1996; Otvos, 2000; Brooke et al., 2008; Scheffers et al., 2011; Tamur, 2012). The established mode for sandy beach ridge formation involves the beach-face receiving sediment transported shoreward resulting in progradation under fair-weather wave conditions (Komar, 1998; Otvos, 2000). As the coastline progrades the beach ridges and inter-dune swales are stranded and preserve a palaeo-environmental record (Tanner, 1988; Otvos, 2000; Tamur, 2012; Taylor and Stone, 1996).

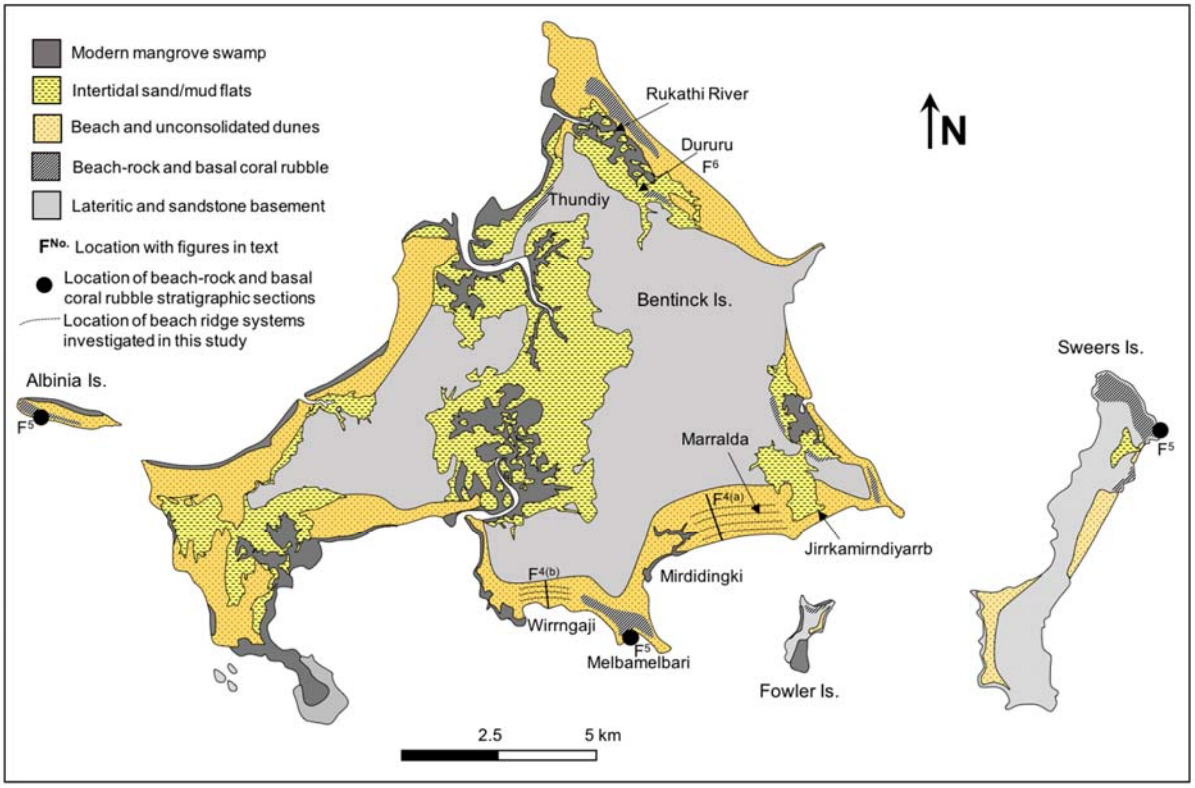

Figure 2: Schematic representation of sea-level index points relative to tidal range in the Gulf of Carpentaria, with a neap tide range of 3 m and spring tide range of 4 m. Transgressive facies within sedimentary successions discussed in results have been included. Grey arrow represents the maximum potential range of the observed proxy. The black box representing the refined indicative meaning based on facies associations.

In contrast to chenier deposits, beach ridges are underlain by near-shore beach sediments and provide an opportunity to investigate palaeo-depositional environments and past sea-level highstands (Otvos, 2000, 2005; Tamur, 2012). However, sea-level studies based on ridge plain elevations and geometry are problematic due to ridges aggrading well above high tide, with significant variations in lateral elevation due to the influence of storm activity (Otvos, 2005; Nott et al., 2013). To use beach ridges as sea-level indicators the boundary between the underlying beach-face with the overlying back-beach deposits, and overlying aeolian facies needs to be correctly identified. The transition between the foreshore (low tide to high tide, and characterized by gentle seaward-dipping planar bedding) and backshore facies (characterized by gentle landward-dipping planar bedding) is formed at the level of landward swash limit of constructive waves, and is regarded as an indicator of the upper tidal level (Otvos, 2000, 2005). In the South Wellesley Islands prograding beach ridge systems are a common feature on Bentinck Island and adjacent mainland (Fig. 3). In this study, an indicative meaning associated with beach ridges as a sea-level proxy is taken from the transition from the beach-face to back-beach deposits (between HWNT and HWST; (*IR*) = +1.5 to +2 m; (*IM)* = +1.75 m; Fig. 2).

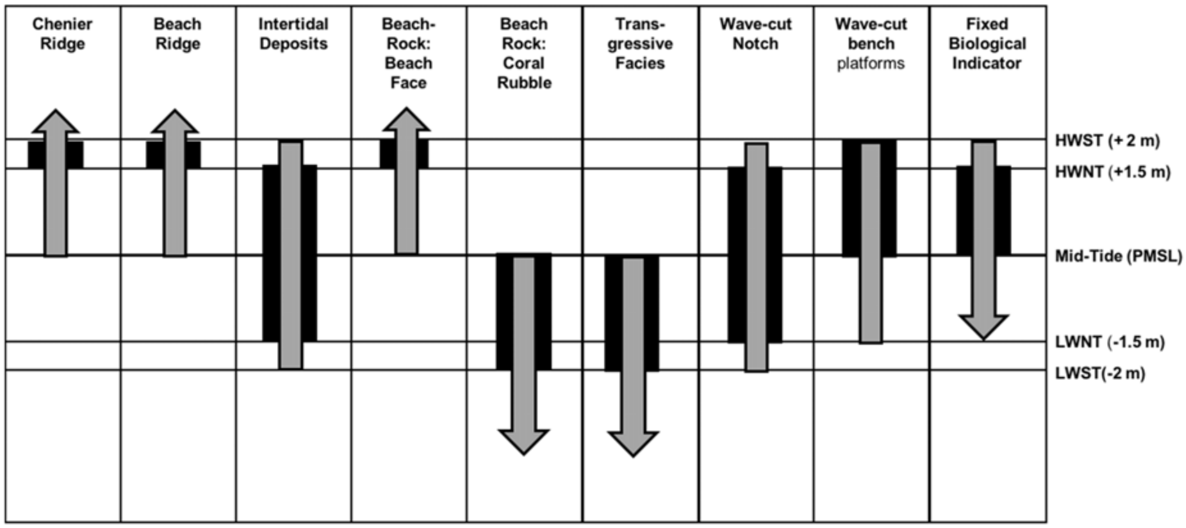

Figure 3: Location and facies map of Bentinck, Sweers, Fowler and Albinia Islands showing various geomorphological features and study sites.

3.1.3 Intertidal and subtidal mangrove and mudflat deposits

Sedimentary successions preserved in intertidal flats (aka. salt/clay pans), and associated mangroves and mangrove sediments, have been used along the southeast coast of Australia as indicators of past sea-level (Grindrod and Rhodes, 1984; Beaman et al., 1994; Grindrod et al. 1999, 2002; Sloss et al., 2005, 2007, 2011; Lewis et al., 2013), as well as globally (Scholl, 1964; Scholl et al 1969; Parkinson 1989; Woodroffe 1981; Hendry and Digerfeldt, 1989). Sedimentary deposits associated with intertidal and mangrove deposits are generally distributed between mid-tide and mean HWNT (Grindrod and Rhodes, 1984; Beaman et al., 1994; Sloss et al., 2007, 2011; Lewis et al., 2013). Accordingly, intertidal and mangrove deposits provide useful indicators of when sea-level attained a particular elevation. However, as with other proxies, intertidal depositional environments are less useful for maximum sea-level as they can be deposited between LWST and HWST. Issues relating to the stratigraphic reliability and precision of such deposits as sea-level indicators have been summarised in Sloss et al. (2007), Smithers, (2011) and Lewis et al. (2013).

Within the South Wellesley Islands mangrove communities are restricted to estuaries and mudflats, forming a coastal fringe within the intertidal zone. Mangrove communities are dominated by *Rhizophora ucronata*, *R. stylosa*, *Avicennia* sp. and *Ceriops tagal* (Saenger and Hopkins, 1975; Saenger, 2005; Rosendahl, 2012; Mackenzie, 2016). Mudflats form extensive features isolated from the open ocean by the mangrove fringe (Figs 2 and 3). The mudflats investigated in this research are now preserved up to 2 m above PMSL and retain a record of coastal landscape evolution over the Holocene. For both mangrove deposits and intertidal mudflats the indicative range is between LWNT and HWNT (*IR* = -1.5 - +1.5 m; *IM* = 0 m; Fig. 2).

3.1.4 Beach-rock

Beach-rock comprises cemented beach sands and is usually found as clearly bedded outcrops of moderately-to-well consolidated sediment, preserving the internal structure of beach facies. The formation of beach-rock has been debated in the literature for several decades, although it is now recognized that it can form through several different processes (see McLean, 2011, and references therein). It is generally agreed that beach-rock forms in the intertidal zone when unconsolidated sediments become lithified by precipitation of aragonite and/or calcite cements, preserving the internal fabric of the beach stratigraphy. Outcrops can be over 3 m thick in areas with relatively high tidal ranges or exposed to high waves/swell conditions (Hopley, 1986; McLean, 2011). While beach-rock may provide a relatively constrained sea-level indicator in micro-tidal environments, the uppermost limit of formation is difficult to determine, particularly in areas with higher tidal ranges (Hopley, 1986; Hopley et al., 2007).

The use of beach-rock as a sea-level indicator is also problematic because it is difficult to determine a precise age for its formation. The constituent grains that formed the beach sand before lithification are almost certain to range across a wide temporal span. Accordingly, the dating of shell material in beach-rock provides a maximum age. Well cemented beach-rock can also undergo several diagenetic phases (Vousdoukas et al., 2007). Consequently, the dating of cements can generate different ages to any biogenic carbonate, providing a minimum age (Desruelles et al., 2009).

Regardless of the issues associated with utilizing beach-rock as sea-level indicators, the facies association between beach-face and back-beach deposits can be used as an indicator of past sea-level (Hopley, 1986; Pirazzoli, 1996). For example, on continental islands in north-eastern Australia, Hopley (1986) determined the vertical error range for beach-rock as a sea-level proxy as the maximum tidal range with an unknown upper level associated with HWST. A more precise sea-level proxy can be established by identifying the boundary between the intertidal beach facies and overlying back-beach and aeolian deposits, restricting the sea-level to the upper intertidal zone (Hopley, 1986; Heartly et al., 2007; Stattegger et al., 2013).

In the South Wellesley Islands extensive partially-to-fully lithified beach-rock coastal outcrops up to 4 m above PMSL provide evidence for coastal deposition associated with the most recent PMT (Figs 2 and 3). The beach-rock deposits preserve sedimentary structures associated with nearshore (beach-face) and backshore facies, and thus provide a sea-level proxy. This transition is equivalent to the modern facies transitions in near-shore and beach successions (between HWNT and HWST; (*IR*) = +1.5 to +2 m; (*IM)* = +1.75 m; Figs 2, 3 and 5). Abundant mollusks associated with the near-shore facies association also provide material for constraining a maximum age for these deposits.

3.1.5 Intertidal erosional indicators

Erosional features that form in the intertidal zone such as wave-cut notches and wave-cut platforms have been used as indicators for past sea-levels in many parts of the world (e.g. Pirazzoli, 1996; Kershaw and Guo, 2001; Benac et al., 2004, Hearty et al., 2007; Smithers, 2011; Rovere et al., 2016). These intertidal erosional features are typically carved into softer rocks such as limestones, and form from a combination of physical weathering (wave action in the intertidal zone), chemical weathering during subaerial exposure during low tide, and biological abrasion (Pirazzoli, 1996; Kershaw and Guo, 2001; Hearty et al., 2007). Wave-cut platforms and notches form around mean sea-level in the intertidal zone and can form over tens to a few hundred years, and thus record previous prolonged sea-level highstands (Pirazzoli, 1986; Neumann and Hearty, 1996; Hearty et al., 2007; Brooke et al., 2017).

Although notches provide geomorphological evidence of former sea-level positions, they can rarely be dated accurately, and can only provide a relative age assessment. In the South Wellesley Islands elevated wave-cut benches and notches are common geomorphological features on exposed rocky coasts (Figs 3, 5 and 6). The wave-cut features have been eroded into the Normanton Formation comprising easily eroded weathered lateritic sandstones and siltstones, or into moderately consolidated beach-rock, and are overlain by late Holocene beach ridges and aeolian deposits. Although these features cannot be dated accurately they do provide geomorphological evidence for past sea-level elevations with modern examples of wave-cut notches occurring between LWNT and HWNT (*IR* = -1.5 – +1.5 m; *IM* = 0 m), and wave-cut benches/platforms between mid-tide and HWST (*IR* = 0 – +2 m, *IM* = +1 m; Figs 2 and 3).

3.1.6 Encrusting organisms and oyster bioherm

Encrusting organisms, such as oysters, tubeworms and barnacles (Fixed Biological Indicators; FBIs), are confined to a restricted range within the intertidal zone on rocky shorelines, and have been utilised as sea-level indicators. For example, relict oyster bed, barnacle and tubeworm deposits have been used to constrain the elevation and duration of the mid-Holocene highstand along the east and west coasts of Australia (Beaman et al., 1994; Baker and Haworth, 1997, 2000a, 2000b; Baker et al., 2001a, 2001b, 2005; Lewis et al., 2008, 2015). A more detailed review of the use of FBIs as proxies for sea-level reconstructions is provided in Sloss et al. (2007) and Lewis et al. (2008, 2013, 2015).

In the Wellesley Islands the encrusting oyster *Striostrea (Parastriostrea) mytiloides* Lamarck, 1819 (common name black-lipped/black-edged oyster), commonly occur on elevated beach-rock deposits, wave-cut benches, and as mono-specific accumulations of bioherm accumulations on exposed mudflats (Rosendahl et al., 2015). *S. mytiloides* is an intertidal species that commonly inhabit water levels from mid-tide to upper-tidal limits (HWNT) attached to rocks and mangrove roots. Therefore, the presence of encrusted *S. mytiloides* on elevated coastal landforms, and the growth of bioherm accumulations provide a sea-level index point from mid-tide to a maximum of HWNT (*IR* = 0 – 1.5 m, IM = +0.75 m; Figs 2-3, 6).

4. Methods

4.1 Field based data: Beach ridges, intertidal and subtidal mudflats, beach-rock and fixed biological indicators.

Augering, D-Section coring, trenches and pits were undertaken to construct stratigraphic sections for beach ridge systems (*n* = 23), intertidal mudflats and mangrove swamps (*n* = 25) and from coastal beach-rock exposures on Bentinck, Sweers and Albinia Islands (*n* = 4; Table 1; Fig. 3). Stratigraphic sections were used to characterize individual facies based on field observations of sedimentary characteristics (grain size, sorting, roundness, lithology), observed sedimentary structures, and faunal elements (Table 1; Figs 3 – 6). Mollusks were collected from stratigraphic sections to identify faunal assemblages, establish their taphonomic history where possible, and for radiocarbon age determination (Sloss et al., 2011). Intertidal erosional indicators comprising wave-cut benches and wave-cut notches on Sweers, Albinia and Fowler Islands were surveyed into Australian Height Datum (AHD; official height datum for Australian which equates to mean sea-level; Geocentric Datum of Australia: Technical Manual, 1998; Umitsu et al., 2001; Sloss et al., 2007; Lewis et al., 2013). Encrusting *Striostrea (Parastriostrea) mytiloides* preserved on elevated wave-cut benches and preserved in beach-rock deposits were collected for radiocarbon dating (Fig. 3; Tables 1, 4 and 5). All stratigraphic sections and wave-cut features were surveyed into ADH. Surveys were conducted using a Real Time Kinematic (RTK) Geographic Positioning Systems (GPS), with a vertical error of approximately 5 cm accuracy.

Table 1: Location and details of auger, pit and stratigraphic sections from the South Wellesley Islands.

Environment	Location	Core Code/ Log Code	Latitude (South)	Longitude (East)	Core AHD (m)	Core depth (cm)
Intertidal mudflats	Thundiy	THU-01	17° 0' 15.9000"	139° 29' 41.5800"	1.60	1.40
		THU-02	17° 0' 48.6000"	139° 29' 40.1400"	1.70	0.80
		THU-03	17° 1' 04.3800"	139° 29' 32.1000"	1.50	0.20
		THU-04	17° 1' 38.2800"	139° 29' 03.7800"	1.60	2.90
		THU-05	17° 1' 46.1400"	139° 28' 43.2600"	1.65	2.20
		THU-06	17° 1' 50.2200"	139° 28' 50.6400"	1.60	3.80
		THU-07	17° 1' 53.1000"	139° 28' 57.4800"	1.60	1.40
		THU-08	17° 1' 54.0600"	139° 27' 27.3600"	1.65	1.55
		THU-09	17° 1' 25.6200"	139° 29' 13.9800"	1.65	2.70
		THU-10	17° 1' 54.4200"	139° 29' 13.9800"	1.60	2.30
		THU-11	17° 1' 54.4200"	139° 29' 13.9800"	1.60	1.45
		THU-12	17° 1' 11.8800"	139° 29' 54.2400"	1.70	1.80
		THU-13	17° 0' 53.5200"	139° 29' 24.4800"	1.75	1.30
		THU-14	17° 1' 52.1400"	139° 29' 37.9800"	1.80	1.50
	Dururu	DUR-01	17° 1' 18.9313"	139° 31' 01.0312"	2.54	2.10
		DUR-02	17° 1' 18.7662"	139° 30’ 59.5375"	2.36	1.70
		DUR-03	17° 1' 15.4739"	139° 30' 57.3336"	1.92	0.40
		DUR-04	17° 1' 17.5051"	139° 30' 59.3162"	2.25	1.90
		DUR-05	17° 1' 19.5595"	139° 31' 01.7808"	2.59	6.00
Beach-ridge system	Marralda	MIR-01	17° 5' 49.6320"	139° 32' 50.8920"	4.90	1.00
		MIR-02	17° 5' 44.0400"	139° 32' 45.9000"	4.20	3.20
		MIR-03	17° 5' 41.9400"	139° 32' 45.9000"	5.80	1.35
		MIR-04	17° 5' 37.4400"	139° 32' 45.6600"	4.20	2.10
		MIR-05	17° 5' 39.3000"	139° 32' 45.6000"	5.15	1.30
		MIR-06	17° 5' 35.7000"	139° 32' 32.6000"	4.45	0.75
		MIR-07	17° 5' 33.1200"	139° 32' 45.2400"	5.30	2.70
		MIR-08	17° 5' 27.8400"	139° 32' 43.9200"	5.75	0.50
		MIR-09	17° 5' 25.3200"	139° 32' 43.9200"	5.85	1.60
		MIR-10	17° 5' 51.2400"	139° 32' 43.9200"	3.80	2.50
		MIR-11	17° 5' 43.3800"	139° 32' 53.7200"	3.30	1.90
		MIR-12	17° 5' 26.2200"	139° 32' 43.8000"	6.50	4.00
		MIR-13	17° 5' 23.9400"	139° 32' 43.8600"	3.50	1.50
		MIR-14	17° 5' 51.6120"	139° 27' 23.0400"	4.25	1.10
	Wirrngaji	WIR-02	17° 6' 48.0000"	139° 29' 10.2000"	4.15	1.00
		WIR-03	17° 6' 51.0600"	139° 29' 13.2000"	4.10	0.80
		WIR-04	17° 6' 52.7400"	139° 29' 15.4800"	4.25	1.40
		WIR-05	17° 6' 55.6400"	139° 29' 17.5200"	3.70	2.40
Beach-rock	Bentinck Is. South	BS1-1A	17° 6' 53.9800"	139° 29' 40.0000"	Stratigraphic	
	Sweers Is. North	SE11	17° 6' 53.9800"	139° 38' 21.8800"	Stratigraphic	
	Albinia Is.	Alb1	17° 1' 19.5400"	139° 12' 45.1600"	Stratigraphic	
Elevated wave-cut bench/notch	Bentinck Is.	N/A	17° 1' 41.5600"	139° 31' 40.8200"	Profile	
	Fowler Is.	N/A	17° 7' 06.3900"	139° 33' 33.2400"	Profile	
	Albinia Is.	N/A	17° 1' 19.5400"	139° 12' 45.1600"	Profile	

4.2 Geochronology

In total 123 previously published radiocarbon (Tables 2b, 3a-c), 15 Uranium Thorium (U-Th; Table 2a), and 5 Thermo and Optical Stimulated Luminescence (TL/OSL; Table 3b) age determinations from the southern and central Gulf of Carpentaria, with an accurate description of facies association and stratigraphic relationship to PMSL (AHD), were calibrated to sidereal years (Table 2a). This includes age determinations from within the central basin by Reeves et al. (2008) who investigated the timing of lowstand lacustrine (non-marine) deposits and fully marine deposits associated with the last full glacial (Reeves et al., 2008, 2013; Table 2a). Previous research by Harris et al. (2008) utilizing U-series dating of drowned coral reefs in the southern Gulf of Carpentaria (Table 2b); and, Rhodes (1982), Rhodes et al., 1980, Nanson et al. (2013) and Rosendahl et al. (2015) age determinations from coastal sedimentary successions (Table 3a – 3c).

An additional 36 AMS radiocarbon age determinations were obtained from the Australian Nuclear Science and Technology Organisation (ANSTO; Hua et al., 2001; Fink et al., 2004) and University of Waikato Radiocarbon Dating Laboratory, New Zealand (Table 4). Radiocarbon age determinations were obtained on samples of fossil marine mollusks and terrestrial organic material. Age determinations were calibrated to sidereal years using the radiocarbon calibration program OxCal v.4.2 (Bronk Ramsey, 2009). Calibration for marine fossil mollusks collected in this study and from previously research used the marine calibration curve (Marine13; Reimer et al., 2013) with a marine reservoir correction for the southern Gulf of Carpentaria ($\Delta R = -49 \pm 102$ yr; Ulm 2006; Ulm et al., 2010) to correct for the marine reservoir effect, and convert ages into sidereal years (expressed as cal. yr BP; Tables 2 – 4; Gillespie, 1977; Gillespie and Polach, 1979; Stuiver et al., 1998; Sloss et al., 2013; Tables 2 – 4). Age calibration for terrestrial samples was performed using the IntCal13 calibration data (Reimer et al., 2013).

Four uranium-series age determinations were undertaken on two coral samples from Sweers Island (Table 4). These samples were selected due to their high percentage of aragonite (>95%) indicating an almost 'closed' system, where minimal diagenesis has occurred. U-Th dates were acquired with multi-collector inductively coupled plasma mass spectrometry (MC-ICP-MS) at the Radiogenic Isotope Facility (RIF), The University of Queensland using method of Leonard et al. (2013), Zhou et al. (2011) and Clark et al. (2012).

All calibrated 14C ages from the previous research and this study are reported as 2σ age range, median and mean ±2σ in cal. yr BP. All TL and OSL ages from the previous research and U-Th ages from this study are also reported as kyr BP. To be compatible with the TL, OSL and U-Th ages, which are shown in mean ages ±2σ, all calibrated 14C ages are also discussed in the text as mean ages ±2σ.

Table 2: Previous published radiocarbon ages from the central Gulf of Carpentaria: (a) Mollusks recovered from cores in the central basin (cf. Fig. 1A; Reeves et al., 2008); and, (b) submerged coral reefs (Harris et al., 2008).

Table 2a.

Environment	Core Code	Core Water Depth (m)	Sample Core Depth (m)	Sample Relative to PMSL (m)	Lab. Code	Conventional 14C age yr BP (1σ)	Calibrated 14C age (cal. yr BP)	
							2σ age range (Median)	Mean±2σ
Non-marine*	MD28	-62	0.6	-62.6	OZG374	10260±80	11715-12392 (12017)	12022±362
	MD31	-59	0.75	-59.8	OZG222	10320±60	11839-12405 (12150)	12160±278
	MD31	-59	0.65	-59.7	OZE251	10350±100	11824-12539 (12202)	12194±374
	MD32	-64	0.35	-64.4	OZF290	10380±70	11997-12527 (12249)	12248±268
	MD30	-60	0.7	-60.7	OZE250	10410±80	12022-12552 (12285)	12284±290
	MD30	-60	0.8	-60.8	OZG231	10430±80	12040-12565 (12311)	12309±292
	MD30	-60	0.9	-60.9	OZG382	10680±70	12445-12732 (12639)	12631±116
	MD31	-59	1.4	-60.4	OZI054	10990±110	12711-13065 (12876)	12881±200
	MD32	-64	0.4	-64.4	OZF291	11440±80	13120-13445 (13282)	13282±170
	MD30	-60	1.5	-61.5	OZF286	11807±170	13305-14052 (13651)	13665±382
	MD32	-64	0.7	-64.7	OZF292	12390±80	14116-14921 (14473)	14490±428
	MD32	-64	1	-65	OZG385	14907±130	17827-18465 (18133)	18136±320
	MD28	-62	0.75	-62.7	OZG375	14280±90	17105-17646 (17391)	17385±280
	MD32	-64	1.45	-65.5	OZG388	14330±100	17130-17752 (17458)	17452±306
	MD32	-64	1.2	-65.2	OZG386	14330±90	17148-17721 (17459)	17453±282
	MD28	-62	0.67	-62.7	OZE254	14350±90	17180-17765 (17486)	17481±284
	MD32	-64	0.75	-64.8	OZG378	14390±80	17272-17818 (17539)	17539±258
	MD33	-68	0.77	-68.8	OZE253	14550±100	17472-17978 (17727)	17726±260
	MD28	-62	0.7	-62.7	OZG373	14960±90	17936-18421 (18183)	18182±248
	MD32	-64	1.5	-65.5	OZF293	15390±110	18412-18877 (18658)	18652±230
	MD33	-68	0.77	-68.8	OZE252	15760±90	18803-19254 (19012)	19023±230
	MD32	-64	2.34	-66.3	OZI055	18320±170	21792-22518 (22173)	22163±380
	MD30	-60	0.6	-60.6	OZF285	9330±70	10295-10710 (10535)	10529±216
Marine mollusks**	MRD28	-62	0.15	-62.2	OZE260	2935±45	2440-3043 (2759)	2752±290
	MRD31	-59	0.1	-59.1	OZF287	10020±160	10565-11695 (11052)	11069±552
	MRD33	-68	0.1	-68.1	OZG237	1310±40	683-1142 (905)	908±234
	MDR30	-60	0.05	-60.1	OZG200	1655±50	1011-1506 (1255)	1253±244

Environment	Core Code	Core Water Depth (m)	Sample Core Depth (m)	Sample Relative to PMSL (m)	Lab. Code	Conventional 14C age yr BP (1σ)	Calibrated 14C age (cal. yr BP)	
							2σ age range (Median)	Mean±2σ
Marine mollusks**	MRD32	-64	0.2	-64.2	OZG384	1820±50	1209-1691 (1427)	1432±240
	MRD31	-59	0.55	-59.6	OZG221	1930±40	1304-1794 (1542)	1544±252
	MRD31	-59	0.3	-59.3	OZG383	2290±45	1705-2270 (1966)	1968±280
	MRD28	-62	0.15	-62.2	OZE261	2600±40	2080-2679 (2353)	2358±310
	MRD33	-68	0	-68	OZG236	2875±45	2356-2928 (2678)	2665±290
	MRD31	-59	0.05	-59.1	OZG220	3770±40	3486-4068 (3770)	3773±290
	MRD31	-59	1.8	-60.8	OZG232	3810±100	3460-4216 (3828)	3833±380
	MRD30	-60	0.65	-60.7	OZE255	4310±60	4188-4816 (4508)	4506±330
	MRD33	-68	0.2	-68.2	OZG258	470±50	0-366 (161)	167±208
	MRD30	-60	0.3	-60.3	OZG381	4860±50	4875-5484 (5212)	5206±312
	MRD31	-59	0	-59	OZE262	6840±50	7178-7588 (7397)	7393±208
	MRD31	-59	0.55	-59.6	OZE256	6910±80	7216-7689 (7459)	7456±234
	MRD33	-68	0.2	-68.2	OZG259	700±30	135-551 (378)	371±202
	MDR31	-59	0.6	-59.6	OZG377	735±35	150-620 (407)	400±198
	MRD28	-62	0	-62	OZE263	750±60	149-637 (418)	411±216
	MRD29	-60	0.05	-60.1	OZF283	820±45	285-652 (482)	475±198
	MRD33	-68	0.3	-68.3	OZG389	820±50	281-656 (482)	475±200
	MRD30	-60	0	-60	OZF284	8270±60	8545-9205 (8865)	8864±336
	MRD28	-62	0.5	-62.5	OZE257	9520±89	10142-10782 (10439)	10443±328
	MRD32	-64	0.1	-64.1	OZG235	9700±45	10371-11011 (10663)	10671±312
	MRD32	-64	0	-64	OZF289	9705±45	10380-11016 (10670)	10678±312
	MRD29	-60	0.2	-60.2	OZE259	9810±90	10488-11148 (10810)	10810±346
	MRD28	-62	0.35	-62.4	OZG379	9920±60	10644-11194 (10932)	10925±294

Table 2: Previous published radiocarbon ages from the central Gulf of Carpentaria: (a) Mollusks recovered from cores in the central basin (cf. Fig. 1A; Reeves et al., 2008); and, (b) submerged coral reefs (Harris et al., 2008).

Table 2b.

Environment	Core Code	Core Water Depth (m)	Sample interval	Sample Relative to PMSL (m)	U-Th age (kyr)
Southern Gulf: Submerged *in situ* corals. Harris et al. (2008).	RD01	-26.8	0.39–0.40	-26.8	9285±77
	RD07	-26.4	0.53–0.54	-26.4	9608±77
	RD08	-29.2	0.37–0.38	-29.2	9661±105
	RD09	-24.4	0.28–0.29	-26.4	8947±62
	RD12	-20.2	0.19–0.20	-20.2	8355±42
	RD12	-20.2	0.90–0.91	-20.2	8506±54
	RD12	-20.2	1.76–1.77	-20.2	9424±53
	RD18	-25.6	0.31–0.32	-25.6	9831±75
	RD27	-29.6	0.15–0.16	-29.6	6966±190
	RD28	-29.2	0.44–0.45	-29.2	9529±111
	RD30	-25.6	0.78–0.79	25.6	9736±13
	RD33	-25.2	0.61–0.62	25.2	7905±10
	RD35	-30.4	0.15–0.16	-30.4	7429±16
	RD37	-24.8	0.53–0.54	-24.8	9505±10
	RD39	-27.6	0.35–0.36	-29.2	9911±40

Table 3: Previous published radiocarbon ages from beach and chenier ridge system and bioherm deposits (a) Rhodes et al., 1980 and Rhodes, 1982; (b) Nanson et al., 2013; and, (c) Rosendahl, 2012 and Rosendahl et al., 2015).

Table 3a.

Location	Sample Material	Lab. Code	Facies	Interface Relative to PMSL (m)	Sample Relative to PMSL (m)	Conventional 14C age yr BP (1σ)	Calibrated ^{14}C age (cal. yr BP)	
							2σ age range (Median)	Mean±2σ
Edward River	Shell Hash	ANU1690	BRdg	1	1.2	6400±90	6629-7249 (6941)	6939±322
Christmas Creek	Shell Hash	ANU1728	BRdg	0.3	1.75	1920±120	1225-1900 (1540)	1547±346
Christmas Creek	Shell Hash	ANU1732	BRdg	1.5	1.5	5370±60	5561-6091 (5791)	5794±262
Christmas Creek	Shell Hash	ANU1734	BRdg	1	1.25	3610±70	3268-3889 (3575)	3578±310
Christmas Creek	Shell Hash	ANU1735	BRdg	1	3.05	3110±65	2710-3290 (2965)	2972±294
Christmas Creek	Shell Hash	ANU1736	BRdg	0.75	3.25	3130±65	2732-3297, 2988)	2994±296
Edward River	*Anadara*	ANU1899	BRdg	0.5	2.1	690±80	80-600 (365)	354±250
Edward River	*Anadara*	ANU2057	BRdg	0.1	1.65	1240±70	624-1109 (838)	844±244
Edward River	Shell Hash	ANU2059	BRdg	0.25	1.75	3300±85	2847-3510 (3192)	3187±332
Edward River	Shell Hash	ANU2060	BRdg	0.55	1.2	3750±80	3417-4089 (3749)	3752±338
Edward River	Shell Hash	ANU2100	BRdg	0.8	1.5	6000±100	6181-6816 (6481)	6486±314
Edward River	*Anadara* and *Mactra*	ANU2101	BRdg	0.6	1	5760±110	5891-6551 (6217)	6214±334
Edward River	Shell Hash	ANU2102	BRdg	0.75	1.75	3430±100	2967-3704 (3353)	3350±364
Edward River	*Anadara*	ANU2103	BRdg	0	1.2	1880±90	1231-1811 (1492)	1500±296
Karumba	*Anadara*	ANU1740A	Chenier	2.75	4.75	5990±90	6186-6776 (6470)	6474±298
Pandanus Yard	Shell Hash	ANU1691	Chenier	2.75	5.4	5830±100	5972-6621 (6297)	6295±322
Karumba	*Anadara*	ANU1740C	Chenier	2.75	4	5780±90	5922-6531 (6239)	6235±306
Karumba	*Anadara* and *Mactra*	ANU1741	Chenier	2	4.4	4260±100	4059-4819 (4437)	4435±396
Karumba	*Mactra*	ANU1742	Chenier	2	2.6	3430±60	3036-3645 (3354)	3350±300
Karumba	*Mactra*	ANU1745	Chenier	1.5	1.95	1080±60	507-911 (696)	702±214
Pandanus Yard	*Mactra*	ANU1827	Chenier	2.35	3.5	2250±60	1615-2240 (1917)	1919±296
Karumba	*Anadara*	ANU1927	Chenier	1.6	2	1770±70	1127-1671 (1379)	1383±262
Karumba	*Mactra*	ANU1928	Chenier	2.25	2.75	2240±65	1597-2240 (1905)	1907±302
Pandanus Yard	*Mactra*	ANU1977	Chenier	1.65	3	680±70	61-560 (358)	347±242
Pandanus Yard	*Mactra*	ANU1998	Chenier	1.65	2.8	550±80	0-444 (231)	232±252
Christmas Creek	Shell Hash	ANU1730	ITM	1.25	1.25	5590±250	5465-6644 (6042)	6045±590
Christmas Creek	Shell Hash	ANU1733	ITM	0.5	0.5	5570±120	5651-6335 (6019)	6014±344
Christmas Creek	Shell Hash	ANU1737	ITM	0.5	0.5	3220±70	2783-3379 (3094)	3094±310
Karumba	*Anadara* and *Mactra*	ANU1743	ITM	1.5	1.5	3840±140	3440-4350 (3874)	3880±460
Edward River	*Anadara*	ANU1898	ITM	0.25	0.25	610±70	0-494 (293)	283±252
Christmas Creek	Shell Hash	ANU1729	STM	0.25	0.25	6160±180	6240-7160 (6668)	6675±472
Karumba	*Mactra*	ANU1744	STM	0.25	0.25	4540±80	4448-5196 (4799)	4801±368
Karumba	*Anadara* and *Mactra*	ANU1746	STM	-1.5	-1.5	3560±70	3209-3829 (3514)	3517±308

Table 3: Previous published radiocarbon ages from beach and chenier ridge system and bioherm deposits (a) Rhodes et al., 1980 and Rhodes, 1982; (b) Nanson et al., 2013; and, (c) Rosendahl, 2012 and Rosendahl et al., 2015).

Table 3b.

Sample Material	**Lab. Code (Core Code)**	**Core Relative to PMSL (m)**	**Facies**	**Interface Relative to PMSL (m)**	**Sample Relative to PMSL (m)**	**^{14}C age BP (1σ)**	**Calibrated ^{14}C age (cal. yr BP)**	
							Median cal. yr BP 2σ range	**Mean cal. yr BP (2σ)**
Mactra sp.	OZM484 (WP171)	0.35	BRdg/C	3.15	1.85	4900±25	4973-5544 (5274)	5261±294
OSL: chenier	AdGL12005 (WP71)	1.38	BRdg/C	3.97	1.4	N/A	N/A	400±30
OSL: chenier	AdGL12003 (WP42)	0.75	Chenier/C	3.1	1.45	N/A	N/A	1520±10
TL: aeolian	W4323 (WP68)	0.5	Chenier/C	3.31	2.11	N/A	N/A	4200±30
Mactra sp.	OZM485 (WP171)	1.65	Chenier/B	1.85	1.85	6250±25	6486-7016 (6761)	6761±260
Anadara antiquata	OZM487 (WP70)	0.90	Chenier	2.15	1.7	1905±35	1287-1764 (1513)	1517±244
Mactra sp.	OZM488 (WP70)	1.05	Chenier/B	2	1.7	1780±30	1169-1617 (1386)	1391±222
TL: chenier	W4324 (WP68)	1.2	Chenier/B	2.61	2.11	N/A	N/A	5700±40
OSL: chenier	AdGL12004 (WP68)	1.2	Chenier/B	2.61	2.11	N/A	N/A	5580±40
Mactra sp.	OZM491 (WP42)	2.40	ITM/DF	1.45	1.45	2140±30	1525-2040 (1782)	1781±258
Bivalve fragment	OZM492 (WP42)	4.35	ITM/DF	-0.5	-0.5	2410±30	1846-2344 (2109)	2108±264
Anadara antiquata	OZM489 (WP70)	2.20	ITM/DF	0.85	0.85	2355±30	1800-2307 (2044)	2046±266

Table 3: Previous published radiocarbon ages from beach and chenier ridge system and bioherm deposits (a) Rhodes et al., 1980 and Rhodes, 1982; (b) Nanson et al., 2013; and, (c) Rosendahl, 2012 and Rosendahl et al., 2015).

Table 3c.

Location	Lab. Code	Facies	Interface Relative to PMSL (m)	Sample Relative to PMSL (m)	^{14}C age BP (1σ)	Calibrated ^{14}C age (cal. yr BP)	
						Median 2σ range	Mean cal yr BP (2σ)
Guttapercha/surface	Wk-23132	FBI	2.76	2.76	4426±42	4370-4935 (4652)	4646±282
Site 36	Wk-38402	FBI	1.34	1.34	4446±30	4402-4941 (4674)	4669±274
Site 12 (Surface)	Wk-23135	FBI	3.3	3.3	5866±45	6092-6610 (6336)	6337±246
Wurdukanhan East	Wk-23133	FBI	1.50	1.50	5142±43	5296-5806 (5547)	5546±254
Site 12	Wk-38404	FBI	3.37	3.37	5576±34	5775-6264 (6029)	6027±244
Site 80	Wk-38405	FBI	1.65	1.65	5899±35	6157-6631 (6370)	6373±234
Site 35	Wk-38406	FBI	1.39	1.39	5913±41	6167-6641 (6384)	6389±240
Site 35 (surface)	Wk-23136	FBI	1.4	1.4	5961±45	6203-6679 (6435)	6439±242
Site 35	Wk-23136	FBI	1.40	1.40	5961±45	6203-6679 (6435)	6439±242
Site 218	Wk-38403	FBI	1.47	1.47	6026±32	6276-6737 (6503)	6505±238
Site 1/A	Wk-38401	FBI	2.93	2.93	6146±37	6385-6900 (6636)	6636±260
Site 1	Wk-23134	FBI	1.50	1.50	6238±47	6459-7021 (6747)	6748±278
Site 1/B	Wk-38407	FBI	2.76	2.76	6246±38	6475-7024 (6756)	7102±270

5. Results

5.1 Geochronology

Radiocarbon ages (*n*=36) were obtained from intertidal mudflat and estuarine successions, beach ridge systems, elevated beach-rock and FBIs. Uranium-series dates (*n*=4) were obtained on two fossil corals (Fig. 3, Table 4). Dating methods, sample location, material/species, laboratory codes, and age determinations are expressed as uncorrected and calibrated ages with their associated error margins (Table 4). Sample elevations, age determinations and associated facies as well as the stratigraphic relationship of specific facies have also been determined relative to PMSL.

5.2 Beach ridge systems (BRdg)

Transects of augers and trenches across a beach ridge system were undertaken at Marralda and Wirrngaji on Bentinck Island. The Marralda/Mirdidingki beach ridge system comprises 10 individual ridges and extends 900 m inland, with an elevation of 3 m to 8 m and an average elevation of 5 m above PMSL. The Wirrngaji beach ridge system comprises 7 individual ridges and extends 500 m inland, elevations from 4 m to 8.75 m, and an average elevation of 4.6 m above PMSL. Three main facies were identified common to both transects (Figs 3 and 4).

1. A basal unit comprising rounded, medium-to-coarse-grained, moderately-sorted mixed siliciclastic and carbonate sand. Faunal elements include present to common disarticulated and rare articulated marine and estuarine bivalves dominated by *Marcia hiantina* and *Gafrarium pectinatum* and the gastropod *Telescopium telescopium* (Table 5). Common to abundant shell fragments, shell hash and rounded-to-well-rounded ironstone pisoliths are common. In trenched sections, low-angled seaward dipping planar beds were observed, often defined by interbedded densely-packed shell beds, shell hash and pisoliths. The facies is interpreted as a beach-face within the beach ridge system (BRdg/BF). A radiocarbon age determination from a reworked *M. hiantina* valve constrains the maximum age for the facies of ca. 5,000 cal. yr BP (Table 4 and 5; Fig. 4).

2. Overlying the basal unit is a fine-to-medium-grained, moderately-sorted siliciclastic quartz sand with a minor component of carbonate shell fragments. Sub-horizontal to very low angled landward dipping planer bedding were observed in trench and pits. Broken disarticulated valves including *M. hiantina*, *Mactra* sp. and *G. pectinatum* are weathered and abraded, shell fragments and shell hash are common. The facies is interpreted as a reworked back-beach deposit (BRdg/BB). Radiocarbon age determinations from re-worked faunal elements indicate and age of ca. 3,500 to 300 cal. yr BP (Tables 4 and 5; Fig. 4).

3. The upper-most facies comprise a well-rounded, well-sorted quartz sand, with common to present pisoliths. Grains are well-frosted and iron-stained indicating reworking and sub-aerial exposure. Shell fragments are present and whole valves rare to present and heavily weather. In places, this facies forms an organic-rich sand with thin (cm-scale) organic-rich humic layer in inter-dune swales. The facies is interpreted as the aeolian capping of the beach ridge system (BRdg/Ae).

Table 4: Age determinations obtained for this study (for site locations see Fig. 1).

Location	Sample Material	Lab. Code	Core Code	Core Elevation (m)	Sample Core Depth (m)	Facies	Sample Relative to PMSL (m)	Facies Interface Relative to PMSL (m)	Conventional 14C Age (yr BP)	Calibrated ^{14}C age (cal yr BP)	
										2σ age range (Median)	Mean±2σ
Bentinck (Rukathi River)	Peat	OZT523	RRB2	NA	N/A	Tf	0.32	0.32	6795±35	7585 - 7681 (7636)	7635±52
Bentinck (Rukathi River)	*Anadara* sp.	OZT524	RRB2-200	NA	N/A	Tf	0.4	0.4	7865±30	8150-8601 (8377)	8377±232
Bentinck (Rukathi River)	*Marcia hiantina*	OZT525	RRB2-230	NA	N/A	Tf	0.66	0.66	6535±30	6830-7325 (7092)	7086±246
Bentinck (Dururu)	*Striostrea mytiloides*	Wk-26684	DUR (surface)	N/A	N/A	FBI	2.11	2.11	4170±40	3979-4609 (4308)	4306±310
Bentinck (Dururu)	*Striostrea mytiloides*	Wk-28768	DUR (surface)	N/A	N/A	FBI	2.21	2.21	4717±42	4776-5321 (5041)	5045±292
Bentinck (Melbamelbari)	*Striostrea mytiloides*	Wk-38839	BS12 (surface)	N/A	N/A	FBI	1.75	1.75	4757±24	4814-5333 (5089)	5087±280
Albinia (South)	*Striostrea mytiloides*	OZT516	A5	N/A	N/A	FBI	2.7	2.7	5185±25	5333-5849 (5598)	5597±242
Sweers (North)	*Favia pallida*	Wk-39387	SE9	N/A	N/A	FBI	1.8	1.8	5652±25	5879-6314 (6102)	6099±230
Bentinck (Marralda)	*Marcia hiantina*	Wk-37071	MIR2.050	4.2	0.5	BRdg/BB	3.7	0.9	1539±25	920-1330 (1138)	1133±214
Bentinck (Marralda)	*Marcia hiantina*	Wk-37072	MIR2.230	4.2	2.3	BRdg/BB	1.9	0.9	1949±25	1327-1808 (1563)	1564±246
Bentinck (Marralda)	*Marcia hiantina*	Wk-37073	MIR10.120	3.8	1.2	BRdg/BB	2.6	1	1229±25	641-1042 (825)	828±204
Bentinck (Marralda)	*Gafrarium (Crista) australe*	Wk-37074	MIR10.230	3.8	2.3	BRdg/BB	1.5	1	1494±25	890-1297 (1096)	1093±214
Bentinck (Marralda)	*Marcia hiantina*	OZT521	MIR10-255	3.8	2.55	BRdg/BB	1.25	1	3620±25	3339-3850 (3584)	3587±264
Bentinck (Wirrngaji)	*Mactra* sp.	OZT529	WIR2-90	4.1	0.9	BRdg/BB	3.2	>3	1695±30	1064-1523 (1299)	1299±228
Bentinck (Wirrngaji)	*Gafrarium (Crista) australe*	OZT530	WIR4-140	4.15	1.4	BRdg/BB	2.75	>2.8	990±30	452-814 (614)	619±176
Bentinck (Wirrngaji)	*Marcia hiantina*	OZT531	WIR5-80	3.7	0.8	BRdg/BB	2.9	0.8	595±30	0-475 (280)	271±234
Bentinck (Wirrngaji)	*Marcia hiantina*	OZT532	WIR5-165	3.7	1.65	BRdg/BB	2.05	0.8	620±30	60-496 (308)	296±230
Bentinck (Wirrngaji)	*Mactra* sp.	OZT533	WIR5-230	3.7	2.3	BRdg/BB	1.4	0.8	455±30	0-330 (148)	154±192
Bentinck (Wirrngaji)	*Marcia hiantina*	OZT522	MIR13-153	3.5	1.53	BRdg/BF	1.97	2.2	4495±30	4436-5011 (4730)	4729±286

Bentinck (Melbamelbari)	*Lumulicardia hemicardium*	Wk-38837	BS1-1a	NA	N/A	BRc/BF	2	2.4	4657±29	4694-5275 (4965)	4973±296
Sweers (North)	*Gafrarium pectinatum*	Wk-39388	SE10	NA	NA	BRc/BB	5	2.3	4786±25	4842-5391 (5121)	5118±282
Sweers (North)	*Gafrarium pectinatum*	Wk-38838	SE11	NA	N/A	BRc/BB	4	2.3	4656±29	4692-5275 (4963)	4972±296
Bentinck (Melbamelbari)	*Gafrarium pectinatum*	Wk-39385	BS4	NA	N/A	BRc/BF	2.88	2.4	3923±25	3680-4275 (3976)	3977±294
Bentinck (Melbamelbari)	*Gafrarium pectinatum*	Wk-39386	BS6	NA	N/A	BRc/BF	3.45	2.4	3902±25	3648-4236 (3947)	3948±294
Bentinck (Thundiy)	*Marcia hiantina*	Wk-37065	THU1.140	1.6	1.4	ITM	0.2	0.2	2721±25	2259-2748 (2506)	2503±262
Bentinck (Thundiy)	*Tegillarca granosa*	Wk-37066	THU4.170	1.6	1.7	ITM	-0.1	-0.1	1553±25	928-1343 (1152)	1146±214
Bentinck (Thundiy)	*Charma* sp.	Wk-37067	THU4.220	1.6	2.2	ITM	-0.6	-0.6	2331±25	1774-2293 (2015)	2017±264
Bentinck (Thundiy)	*Charma* sp.	Wk-37068	THU4.290	1.6	2.9	ITM	-1.3	-1.3	3670±25	3380-3906 (3646)	3648±268
Bentinck (Thundiy)	*Gafrarium (Crista) australe*	OZT526	THU6-380	1.6	3.8	ITM	-2.2	-2.2	1435±20	819-1257 (1039)	1039±220
Bentinck (Thundiy)	*Marcia hiantina*	Wk-37069	THU7.140	1.6	1.4	ITM	0.2	0.2	4020±25	3830-4399 (4108)	4108±296
Bentinck (Thundiy)	*Marcia hiantina*	OZT527	THU11-140	1.6	1.4	STM	0.2	0.2	4145±25	3969-4557 (4275)	4272±294
Bentinck (Dururu)	*Gafrarium (Crista) australe*	Wk-37070	DUR1A.170	2.54	1.7	STM	0.84	0.84	6038±25	6285-6742 (6516)	6517±236
Sweers (North)	U/Th: Coral - *Faviidae*	WZ08_47	SE6 (i)	NA	N/A	Ae	6.1	6.1	N/A	N/A	5973±14
Sweers (North)	U/Th: Coral - *Faviidae*	WZ08_48	SE6 (ii)	NA	N/A	Ae	6.1	6.1	N/A	N/A	5878±76
Sweers (North)	U/Th: Coral - *Faviidae*	WZ08_49	SE1 (i)	NA	N/A	Ae	6.1	6.1	N/A	N/A	5706±11
Sweers (North)	U/Th: Coral - *Faviidae*	WZ08_50	SE1 (ii)	NA	N/A	Ae	6.1	6.1	N/A	N/A	5713±13
Sweers (North)	Coral - *Faviidae*	Wk-40373	SE6 (i)	NA	N/A	Ae	6.1	6.1	5578 ± 20	5789-6264 (6031)	6029±236
Sweers (North)	Coral - *Faviidae*	Wk-40374	SE6 (ii)	NA	N/A	Ae	6.1	6.1	5574 ± 20	5785-6260 (6027)	6025±238
Sweers (North)	Coral - *Faviidae*	Wk-40375	SE1 (i)	NA	N/A	Ae	6.1	6.1	5487 ± 20	5679-6175 (5925)	5926±256
Sweers (North)	Coral - *Faviidae*	Wk-40376	SE1 (ii)	NA	N/A	Ae	6.1	6.1	5520 ± 20	5713-6205 (5966)	5966±252

Figure 4: Profiles from Marralda and Wirrngaji and representative composite stratigraphic section of coastal beach ridge systems.

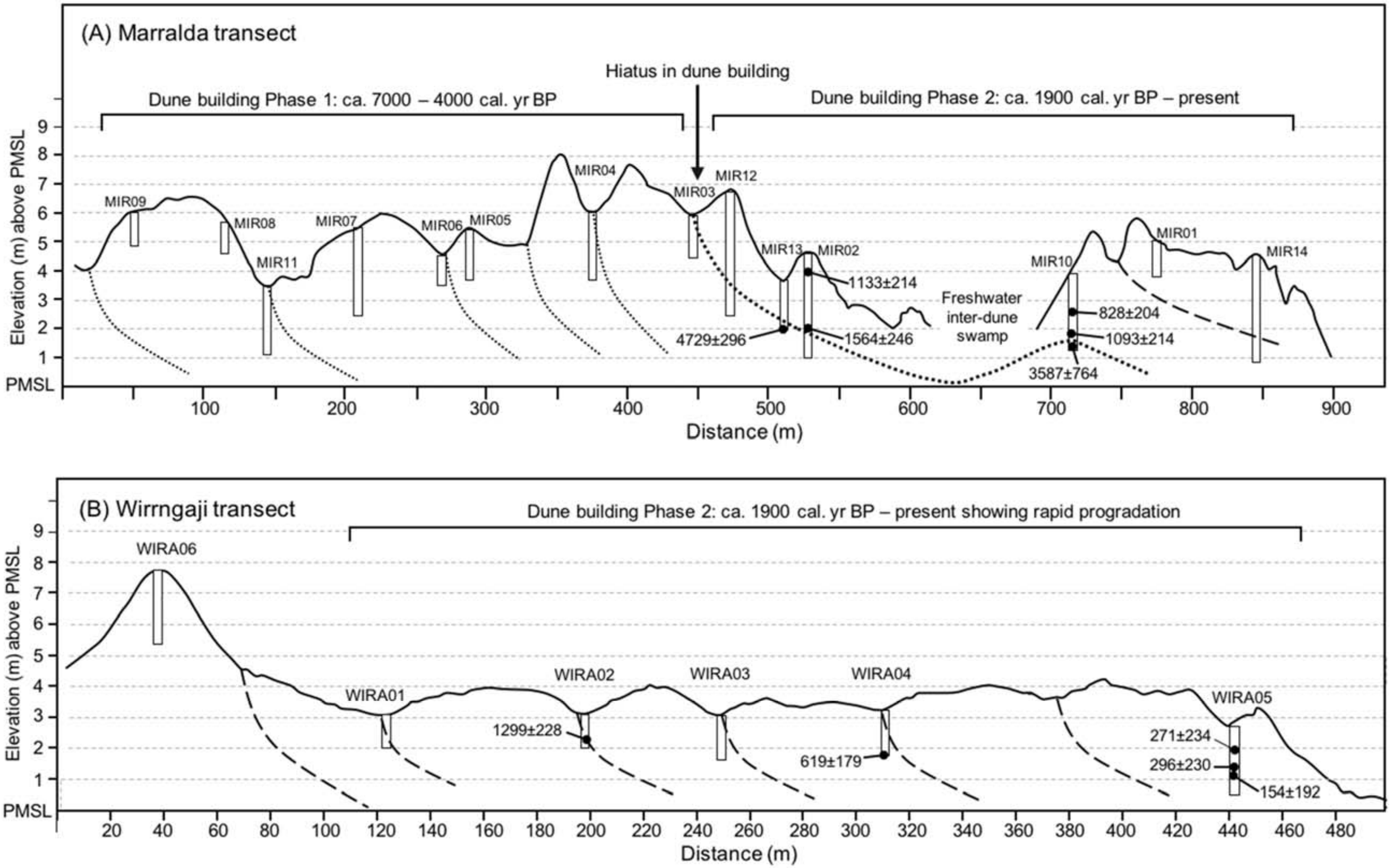

Table 5: Relative abundance of faunal elements relative to facies associations. Habitat information from Hodgson (1998) and Carpenter and Niem (1998). a = absent; R = rare; P = present; C = common; VC = very common; F = fragments and/or shell hash.

	Faunal Element	Original Habitat	Facies			
			Trans-gressive Facies	Intertidal Facies	Beach Rock Facies	Beach Ridge System
Bivalves	*Tegillarca granosa (Anadara granosa)* Linnaeus, 1758	Common on muddy to muddy sand substrates, mainly in protected bays, estuaries, and mangroves environments. Intertidal (optimal water depths of 1-2 m either side of mid-tide), inhabiting environments with relatively low salinity.	*C (F-C)*	*VC*	*P*	*P (F-C)*
	Chama pacifica Broderip, 1834	Attached to corals, rocks, and pebbles. Littoral and sublittoral to a depth of 30 m.	*P*	*C*	*P*	*P*
	Circe scripta Linnaeus, 1758	Sandy substrates in the intertidal and shallow subtidal to a depth of about 20 m.	*P*	*C*	*P*	
	Fragum hemicardium Linnaeus, 1758	Common in intertidal sandy substrates associated with sandflats of sheltered bays.	*C*	*VC*	*C*	*P*
	Gafrarium pectinatum Röding, 1798	Sandy substrates in intertidal and subtidal environments to a depth of ca. 30 m.	*VC*	*VC*	*C (F-C)*	*P-C*
	Lunulicardia hemicardium Linnaeus, 1758	Abundant in intertidal sandflats of sheltered bays with a depth range of 0 - 5 m.	*VC*	*C*	*C*	*R*
	Mactra maculata Gmelin, 1791	Fine sandy substrates in intertidal and subtidal environments (up to 60 m water depth).	*C*	*C*	*C (F-C)*	*P-C*
	Marcia hiantina (Katelysia hiantina) Lamarck, 1818.	Sandy to silty substrates in sheltered intertidal areas to subtidal up to 20 m water depth.	*C*	*C*	*P*	*R*
	Geloina erosa Lightfoot, 1786	Muddy substrates in fresh and brackish waters associated with mangrove swamps and estuaries. Can survive sub-aerial exposure for a few days.	*P*	*P*	*a*	*a*
	Saccostrea cuccullata Born, 1778	Attached to various hard substrates in the intertidal zone (max. depth 5 m) associated with estuarine and mangrove environments.	*VC*	*a*	*a*	*a*
Gastropods	*Pollia undosa (Cantharus undosus)* Linnaeus, 1758	Intertidal on rocky or sandy substrates, also found associated with dead corals, in reef areas.	*P*	*C*	*a*	*a*
	Cerithium coralium Kiener, 1841	Found in the upper tidal zone (mid-to-high-tide) mudflats of estuarine and mangrove areas.	*P*	*C*	*C (F-C)*	*R*
	Clypeomorus batillariaeformis Habe and Kosuge, 1966	Sandy substrates in the intertidal zone associated with reef flats and estuarine environments.	*P*	*P*	*R*	*a*
	Littoraria scabra Linnaeus, 1758	Found attached to trees, roots and pneumatophores at the seaward edge of mangrove environments. Can also be found on sandy shores and on sheltered rocky intertidal environments.	*P*	*C*	*a*	*a*

	Rhinoclavis vertagus Linnaeus, 1758	Abundant on sandy substrates in intertidal and sub-tidal environments to a depth of ca. 13 m.	*P*	*P*	*R*	*R*
	Terebralia sulcata Born, 1778	Common on mudflats in estuaries and mangrove environments, often attached to pneumatophores and roots of the trees.	*P*	*C*	*P*	*R*
	Telescopium telescopium Linnaeus, 1758	Abundant in mangrove areas and on intertidal mudflats in saline or highly brackish environments.	*VC*	*VC*	*C*	*P-C*
Corals	*Acropora formosa* (Dana, 1846)	often dominate large areas of lagoon in shallow and intermediate depths.	*VC*	*a*	*P*	*a*
	Acropora humilis (Dana, 1846)	found on exposed reefs throughout its range in shallow to intermediate depths.	*C*	*a*	*a*	*a*
	Acropora palifera (Lamarck, 1816)	Common in shallow to intermediate depths and wave-washed environments.	*VC*	*a*	*a*	*a*
	Favia favus (Forsskål, 1775)	found at all depths	*VC*	*a*	*P*	*a*
	Heliopora coerulea (Pallas, 1766)	Most common in shallow water.	*C*	*a*	*a*	*a*
	Pectinia lactuca (Pallas, 1766)	Common from below the reef flat to the limit of coral growth.	*C*	*a*	*a*	*a*
	Platygyra daedalea (Ellis and Solanader, 1786)	Colonies commonly grow to 1 m diameter or more and are found at all depths.	*C*	*a*	*a*	*a*

5.3 Intertidal and subtidal mangrove and mudflat deposits

Cores and trenches in supra-tidal mudflats on Bentinck Island that are now elevated above PMSL (max. elevation +2.8 m above PMSL) intersected sediments associated with intertidal mudflats and mangrove deposits, overlying heavily weathered Winton Formation (Fig. 5). Stratigraphic sections along two transects (at Durruru and Thundiy) revealed four facies.

1. The basal mottled dense clay representing the weathered Winton Formation (Fig. 5).

2. In places (laterally discontinuous) medium-grained, mixed siliciclastic and carbonate muddy sand. Faunal assemblage includes common articulated and disarticulated estuarine and nearshore mollusks including bivalves species identified in beach ridge systems as well as *Tegillarca granosa*, *Lunulicardia hemicardium*, *M. hiantina*, and *Mactra* sp., as well as common gastropods *Pollia undosa*, *Cerithium coralium* and *T. telescopium.* The facies is interpreted as a transgressive facies (Tf). At Rukathi River this facies contains densely-packed, centimetre-thick, organic-rich interbeds, representing intertidal mangrove facies. Radiocarbon age determination returned ages of 8,377±227, 7,611±187 and 7,092±262 cal. yr BP (Table 4).

3. Organic-rich sub-rounded-to-rounded fine-to-medium-grained silty sand (quartz). Common to abundant estuarine and nearshore bivalves *T. granosa*, *L. hemicardium* and *M. hiantina*, as well as common gastropods *P. undosa*, *C. coralium* and *T. telescopium*. Radiocarbon age determinations on an estuarine bivalve range from ca. 4,000 to 1,000 cal. yr BP (Table 4). Fine laminations are observed in pits and trench sections. This facies is interpreted as an intertidal mudflat (ITM).

4. The upper-most facies comprises very fine-grained silty sand. Fine laminations are observed in pits and trench sections. Salt crusts and desecration structures are common at the surface. This facies is interpreted as the modern supra-tidal mudflat.

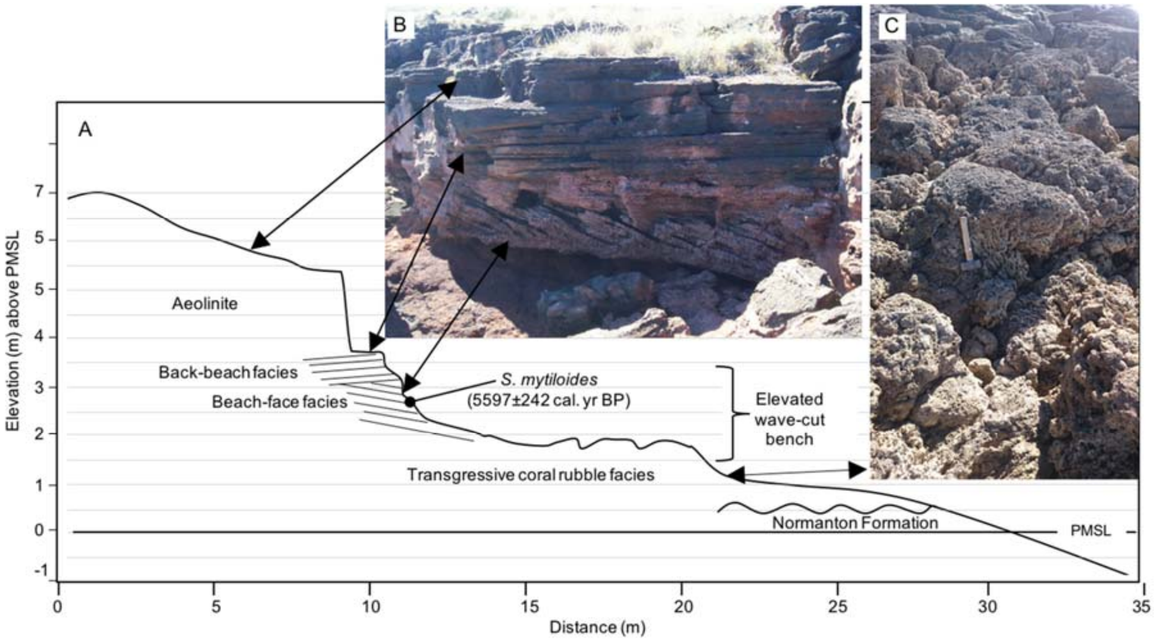

Figure 5: Representative profile and composite stratigraphic section of beach-rock outcrop identified on Bentinck, Sweers and Albinia Islands. (A) Profile of wave cut bench into beach-rock deposits on Albinia Island; (B) example of transition between seaward dipping (beach-face) and landward dipping (back-beach) planar bedding preserved in beach rock-deposits on Albinia Island; and, (C) example of in situ and reworked coral rubble associated with the most recent PMT on Sweers Island.

5.4 Beach-rock

Stratigraphic logging of coastal exposures of beach-rock deposits from Albinia, Bentinck and Sweers Islands resulted in the identification five main facies (Figs 3, 5 and 6).

1. Lower Cretaceous Normanton Formation comprising lateritic bedrock and weathered siltstones. Generally, highly-weathered producing a mottled orange/red/white fine-grained siltstone, commonly forming wave-cut cliffs and platforms in coastal outcrop. The Normanton Formation forms the basal unit (bedrock) and core of the South Wellesley Islands.

2. A laterally discontinuous unit ranging from a few centimetres to 30 cm-thick. This facies comprises coral rubble in a medium-to-very-coarse-grained sand matrix and reworked shelley rubble with grainstone or boundstone texture and a sharp unconformable contact with the lateritic bedrock. This unit includes fragmented and reworked whole corals (*Favia favus and Acropora* sp.), abundant gastropods (*T. telescopium*) and bivalves (*G. australe*). Present-to-common *in situ* coral occur at the base of the coral rubble facies. The facies is interpreted as transgressive facies (Coral/TF). Radiocarbon age determinations could not be obtained on *in situ* coral due to recrystallization, however radiocarbon and U-Th ages from reworked coral do provide an age constraint of ca. 6,000 cal. yr BP (Table 4; Fig. 3, 5 and 6).

3. Consolidated beach-rock deposits unconformably overlying the lateritic bedrock. The facies is characterized by a mixed siliciclastic and bioclastic sediment with individual units generally fining-up from gravel and coarse-grained grainstone to medium-grained grainstone. Tabular forest beds with an east-west strike and dips varying between horizontal to ~25° to the south (seaward) are well-preserved. Faunal elements within this facies include heavily fragmented abundant gastropods (*Terebralia* sp., *Calliostoma* sp.) and bivalves (*G. pectinatum, G. australe, L. hemicardium*). The facies is interpreted as beach-face facies (BRc/BF; 5 and 6).

4. Up sequence the BRc/BF facies grades to a poorly-consolidated beach-rock characterized by a graded coarse-grained grainstone, fining-up to a fine-grained grainstone. The facies is characterized by low angle planar bedding with a southeast-northwest strike and a northeast (landward) dip angle of 11°- 28°. Faunal elements include very abundant fragmented gastropods (*Terebralia* sp., *Calliostoma* sp.) and bivalves (*G. pectinatum, G. australe, L. hemicardium*). The facies is interpreted as a back-beach facies (BRc/BB). Radiocarbon age determinations from this facies range from 5,100 to ca. 4,000 cal. yr BP (Table 4; 5 and 6).

5. Aeolianite Facies: The aeolianite deposits are partially consolidated very fine-to-medium-grained, poorly-sorted, sub-angular-to-sub-rounded siliciclastic and bioclastic sediments. The aeolianite facies is a laterally variable unit reaching up to 2 m-thick in some sections, with a sharp basal contact with the underlying beach-rock and a distinct karstic weathering. Faunal elements included rare-to-present fragmented bivalves (*G. pectinatum, G. australe, L. hemicardium*) and very rare-to-rare gastropods (*Terebralia* sp., *Calliostoma* sp.). Within the aeolianite facies corals (*F. pallida, L. phyrgia*, *Heliopora coerulea, C. serailia*) ranging in size from 6 to 13 cm occur as reworked and imbricated concentrated bands.

5.5 Intertidal erosional indicators

Wave-cut notches and benches eroded into the soft weathered lateritic sandstones and siltstones of Normanton Formation are common geomorphological features on the South Wellesley Islands. These erosional features are commonly overlain by Holocene deposits and/or aeolian dunes containing archaeological material. These features are hypothesised to represent the elevation of the Holocene highstand eroded into the soft bedrock and/or moderately consolidated beach-rock. The wave-cut bench surveyed on Fowler Island extends up to 4 m horizontally, eroded into the Normanton Formation. The wave-cut benches surveyed on Albinia and Sweers Islands extends between 10 – 20 m horizontally, eroded into beach-rock deposits (Fig. 6). These wave-cut features have a consistent elevation (*IM*) of between +1.5 and +3.5 m (Avg. elevation = +2 m). On Bentinck Island a wave-cut notch of ca. +1.5 m in height and 1.5 m in depth occupies the upper limits of the elevated intertidal mudflats at Rukathi River at an elevation of between +1.5 and +2.5 m above PMSL indicating a contemporary sea-level (*IM*) of ca. 2m above PMSL (Fig. 5 and 6).

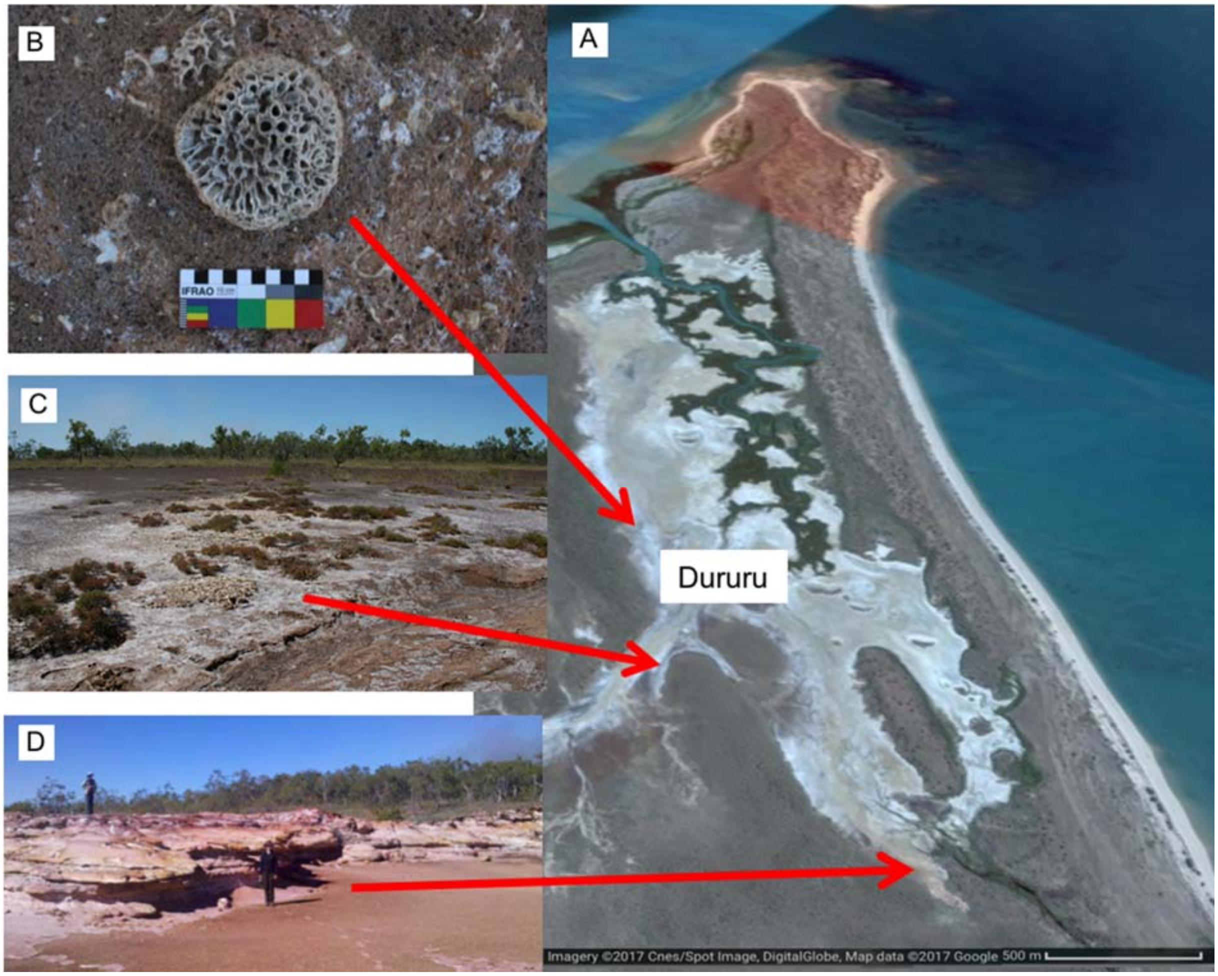

Figure 6: Representative profile of intertidal successions at Rukathi River and location of examples of various sea-level proxies utilized in this research. (A) Rukathi River supratidal mudflats; (B) in situ coral head preserved in partially consolidated beach-rock deposits at Dururu; (C) elevated accumulation of in situ S. mytiloides overlying partially consolidated beach-rock deposits at Dururu; and, (D) Wave-cut notch into Normanton Formation.

5.6 Encrusting organisms and Oyster bioherm

On both Bentinck and Albinia *S. mytiloides* occur as small accumulations attached to elevated wave-cut benches and within partially consolidated deposits. On Bentinck Island *in situ S. mytiloides* were recovered at the landward margin of the extensive intertidal and supra-tidal mudflats at Dururu. Age determinations on *in situ S. mytiloides* recovered from the lowest elevation returned a radiocarbon age of 4,295±315 cal. yr BP (*IM* +1.36 m, Table 4). At the upper limit *in situ S. mytiloides* returned a radiocarbon age of 5,050±271 cal. yr BP (*IM* +1.46 m; Table 4). Encrusted *in situ S. mytiloides* collected from the raised notches on Albinia and the coral rubble facies on Bentinck returned radiocarbon age determinations of 5,998±265 at +1.95 m, and 5,100±223 m at +1 m respectively (Table 4).

6 Discussion: Revised sea-level history for the southern Gulf of Carpentaria

Utilizing results from previous studies and from this research a detailed history of Holocene sea-level change has been constructed for the southern Gulf of Carpentaria. The sea-level history has been divided into three main phases. The first phase extends from when sea-level first inundated the Gulf of Carpentaria region until the culmination of the most recent PMT (ca. 12,000 – 7,700 cal. yr BP). The second phase includes the mid-Holocene sea-level highstand that extended from ca. 7,000 to 4,000 cal. yr BP. The third phase includes the sea-level regression from ca. 4,000 cal. yr BP until the present (Fig. 7). Each phase is characterised by a specific set of climate conditions and sea-level elevation which significantly influenced coastal landscape evolution.

6.1 Phase 1: Post-glacial marine transgression of the Gulf region (ca. 12,000 – 7,700 cal. yr BP).

The compilation of previous research, with results from this study, indicate that sea-level rose from -53 m (depth of the Arafura Sill) ca. 11,700 years ago to ca. -25 m by 9,800 years ago (Fig. 8). Based on results from *in situ S. mytiloides* and transgressive deposits sea-level attained PMSL by 7,700 years ago and continued to rise to an elevation of between 1.5 and 2 m by 7,000 years ago. The revised sea-level history contrast with previous research that suggest a much higher sea-level of ca. 2.5 m above PMSL ca. 6,400 cal. yr BP (Rhodes 1982; Chappell et al., 1982; Rhodes et al., 1980). Results from this research also place the culmination of the most recent PMT 2,000 to 1,500 years earlier than previously reported (Rhodes, 1980, Chappell et al. 1982, Rhodes et al., 1982). A recalculation of the rate of sea-level rise indicates an initial rapid rise of 12.73 m/ka following inundation 12,000 years ago (Fig. 8). The rate of rise decreased to 11.36 m/ka as sea-level approached PMSL, and slowed dramatically to 1.09 m/ka during the culmination of the most recent PMT as sea-level peaked between 7,000 and 6,500 cal. yr BP.

Rising sea levels attained present levels ca. 7,700 years ago and attained an elevation of between +1.5 and +2 m by ca. 7,000 cal. yr BP (Figs 7 and 8). This contrasts to previous research in the southern Gulf of Carpentaria that suggested the culmination of the most recent PMT rose to present levels between 6,500 and 6,000 years (rate of rise = 12 m/ka) and continued to rise to a highstand of approx. +2.5 m ca. 6,000 – 5,500 yr BP, before falling smoothly to its present level (Rhodes, 1980; Chappell *et al*., 1982; Rhodes *et al*., 1982; Chappell and Thom 1986). This is a critical data set as Chappell *et al*. (1982) used the observational data from the Karumba chenier ridges to ‘calibrate’ the hydro-isostatic model for northern Australia.

Results demonstrate an earlier culmination of the most recent PMT, and an alternate history of highstand and regression over the mid-to-late Holocene. While coastal erosional features are difficult to date, the wave-cut notches and benches surveyed in the South Wellesley Islands provide evidence to support the hypothesis that they formed during the most recent PMT. For example, at the landward limit the erosional bench on Fowler Island is overlain by Holocene dune sediments that contain evidence of human occupation dated to between 132 cal. yr BP (431±25 BP, Wk-34781) and 934 cal. yr BP (1,337±25 BP, Wk-34783). The weathered Normanton Formation is a soft laterite and easily eroded, making it unlikely that wave-cut features are remnants of previous interglacials. Using the modern platform as an analogue the elevated wave-cut notch and benches represent an elevated sea-level of 2.25±1.5 m above PMSL, most likely formed during the culmination of the most recent PMT (Figs 5 and 6)

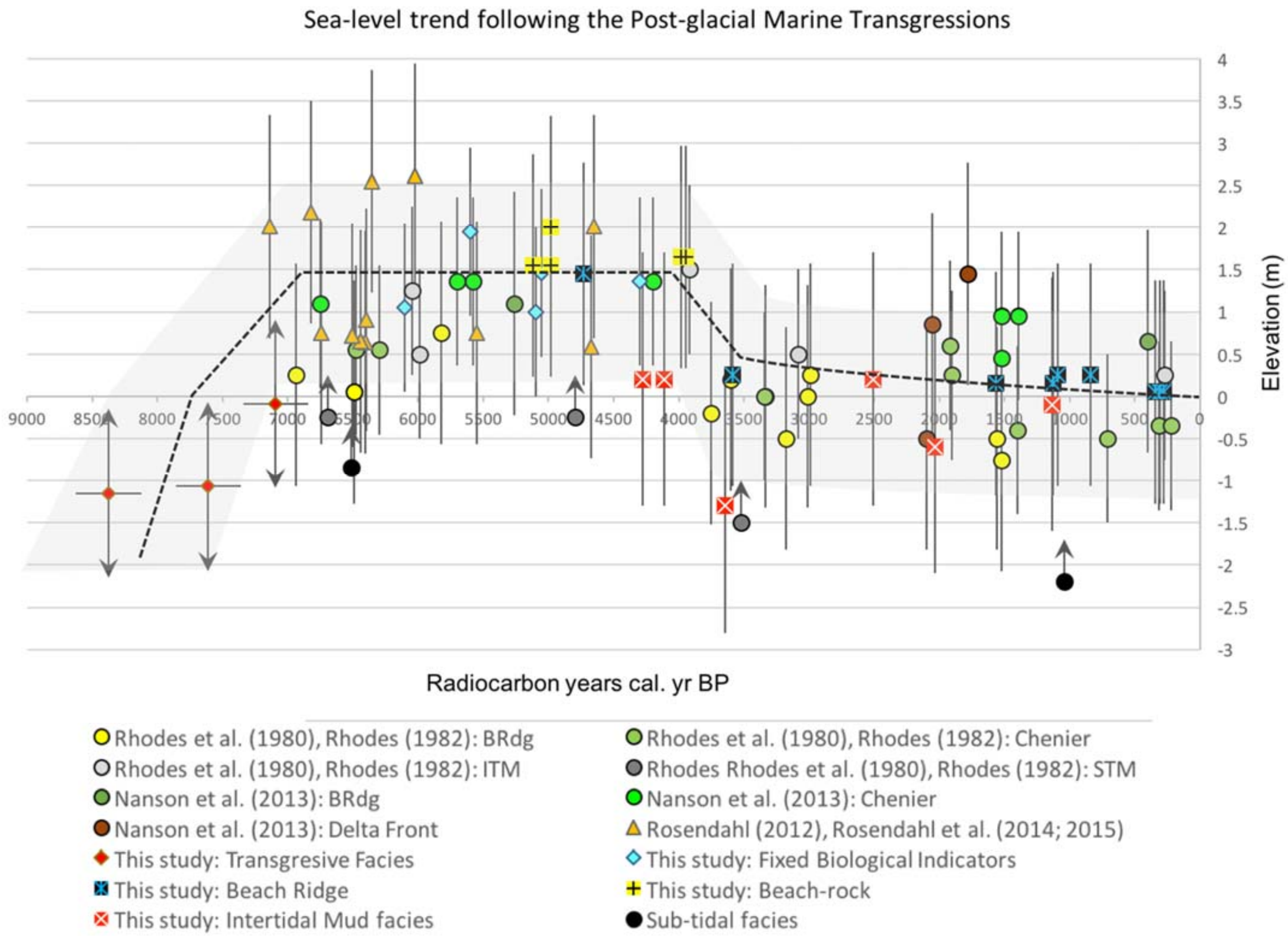

Figure 7: Revised Holocene sea-level curve for the southern Gulf of Carpentaria 10ka - present. Sea-level curve representing line of best fit through the data points; grey hash represents the averaged vertical error of sea-level proxies and incorporates age determination errors.

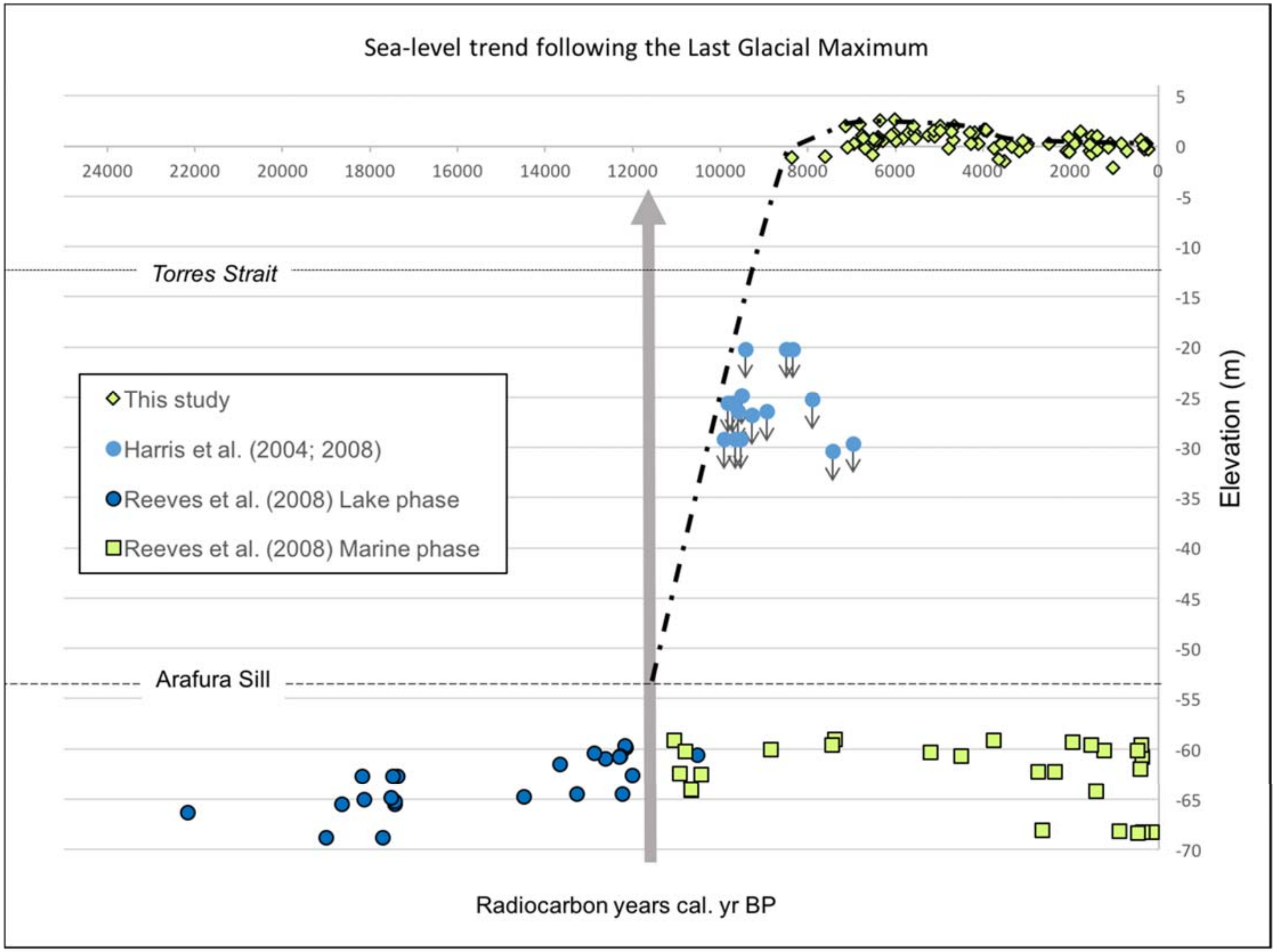

Figure 8: Revised Holocene sea-level curve for the southern Gulf of Carpentaria 22 ka - present.

A more accurate elevation and age control for sea levels during the most recent PMT has been obtained utilizing fixed biological indicators. On Mornington Island 12 *S. mytiloides* bioherm clusters were documented by Rosendahl et al. (2015). The bioherm clusters are characterized by mono-specific accumulations of *S. mytiloides* that exhibit excellent valve preservation and an abundance of articulated valves representing *in situ* accumulation. Radiocarbon age determinations from the bioherms fall between and 7,000 and 4,600 cal. yr BP at elevations between 1.34 and 3.3 m above PMSL (Table 4). The age determinations obtained from five bioherms from Mornington Island reported by Rosendahl et al. (2015) indicate that the coastline was adjacent to the bedrock margins by ca. 7,000 cal. yr BP and embayments represented both inter- and subtidal environments characterized by sea-grass beds and mangrove communities, and not a supra-tidal mudflat as it is today.

Age determinations on *in situ S. mytiloides* from this study are consistent with Rosendahl et al. (2015). *S. mytiloides* attached to wave-cut features from Albinia, Sweers and Bentinck Islands show that sea-level was between +1 to +1.95 (*IM*) above PMSL by 6,100±217 cal. yr BP. Further evidence constraining the timing of the culmination of the most recent PMT was recovered from transgressive deposits associated with a basal coral deposit underlying late Holocene deposits. An *in situ S. mytiloides* within the basal coral rubble facies indicates that the transgressive facies was deposited before 5,100 cal. yr BP. U-Th and radiocarbon age determinations on the re-worked corals in storm deposits preserved within the overlying aeolian facies indicate that coral communities would have been in growth position near present sea-level ≥ 6,000 cal. yr BP, and subsequently been incorporated into the overlying aeolian facies. Results utilizing FBIs from Rosendahl et al., (2015) and results from this study indicate that sea-level attained PMSL by 7,700 cal. yr BP, continued to rise to between 1.5 and 2 m above PMSL by between 7,000 and 6,500 cal. yr BP (Table 4; Fig. 7).

Similar evidence for the timing and elevation of the culmination of the most recent PMT were obtained from transgressive mangrove deposits. Since mangrove-related sedimentary deposits are intertidal, occupation at a particular level in the past can provide an indication of the position of former sea-level (Jones et al., 1979; Thom and Roy, 1983, 1985; Woodroffe, 1988; Sloss et al., 2005, 2007; Lewis et al., 2013). On the Wellesley Islands transgressive mangrove muds occur beneath intertidal mudflats which records both changes of sea-level and coastal landscape response to such changes. Within the transgressive deposits at Rukathi a dense shell bed was dated at 8,377±227 cal. yr BP. This unit has sharp upper and basal contacts with abundant disarticulated and hydro-dynamically sorted bivalves. This is most likely a storm-redeposited bed within an early forming mangrove fringe, however, the age determination still indicates that sea-level was close to present ca. 8300 years ago to have been able to supply re-worked material into the nearshore zone. Additional results from transgressive deposits indicate that sea-level attained PMSL between 7,611±187 and 7,092±262 cal. yr BP (Table 4; Fig. 7).

6.2 Phase 2: Mid-Holocene sea-level highstand (ca. 7,000 – 4,000 cal. yr BP)

Following the culmination of the most recent PMT sea-level remained at an elevation of between 1 – 2 m above PMSL during the Holocene highstand which lasted until ca. 4,000 cal. yr BP. For example, results from the landward limit of the Dururu claypan show that *in situ S. mytiloides* clusters accumulated between 5,050±217 cal. yr BP (upper limit of oyster bed +1.46 m) and 4,295±315 cal. yr BP (lower limit of oyster bed +1.36 m). It was also during this phase of elevated sea-level that resulted in the formation of successions. Environmental conditions were favorable with increased temperatures and precipitation during the mid-Holocene, climate optimum (Shulmeister and Lees, 1992; Shulmeister, 1999), facilitating dissolution and precipitation of carbonate material, resulting in the formation of beach-rock immediately following the culmination of the most recent PMT. Results from this research identified the facies interface between the shallow seaward dipping and landward dipping beach facies to be between 2 and 2.4 m above PMSL. Radiocarbon age determinations from reworked bivalves provide a maximum age for the deposit and indicate that they were forming ≥ 5,100 years ago, and abruptly ceased formation shortly after 4,000 cal. yr BP (Figs 7 and 8; Table 4). The cessation of beach-rock formation is most likely associated with a decrease in effective precipitation and temperature after ca. 5,000 years ago (Shulmeister and Lees, 1992; Shulmeister, 1999), and a falling sea-level from 4,000 cal. yr BP resulting in a decrease in accommodation and sediment supply.

Increased precipitation and temperature combined with elevated sea levels during the Holocene sea-level highstand also had a significant influence on chenier and beach ridge initiation and development. Beach ridge systems at both Marralda and Wirrngaji show general age progression from the older landward dunes to the younger seaward dunes with results indicating an initial phase of dune building associated with the culmination of the most recent PMT ca. 6,700 – 6,000 cal. yr BP (Fig. 7). Increased dune activity would have been facilitated by increased sediment supply associated with higher effective precipitation. Increased sediment supply, combined with elevated sea-levels of between 1.5 and 2 m above PMSL, and increased accommodation in the near-shore environment resulted in the accretion of elevated beach and chenier ridges at the landward limits. Results from this study are consistent with similar geomorphological evidence on Groote Eylandt, the Cobourg Peninsula (northeast of Darwin) and Cape Flattery on Cape York Peninsula, that indicate coastal dune initialization and stabilization occurring between 6,000 to 4,000 years ago (Lees 1987; Lees et al., 1990; Shulmeister and Lees, 1992). It was this phase of elevated sea-levels associated with the highstand that resulted in the initiation and development mangrove and intertidal flats. Radiocarbon age determinations from fossil mollusks recovered from mangrove and intertidal flats indicate that they were established by 4,000 years ago (Fig. 7; Table 4).

6.3 Phase 3: Regression from mid-Holocene sea-level highstand to present mean sea-level (ca. 4,000 cal. yr BP – present)

A second phase of ridge development occurred between 3,700 and 3,000 years ago (in contrast to a 4,500 – 2,900 ^{14}C phase promoted by Rhodes, 1982). This second phase of dune activity is characterised by lower elevations of dune and chenier ridges (Figs 4 and 7). In contrast to higher dune accretion of Phase 1, this phase of dune and chenier development is characterised by accelerated coastal progradation due to a loss of accommodation associated with falling sea-levels from ca. 4,000 years ago (Fig. 7).

Results indicate a potential hiatus in coastal accretion between 3,000 and 1,900 cal. yr BP. Again, results from this research are consistent with research by Lees (1987) and Lees *et al*. (1990), Shulmeister and Lees (1992) who identified a sharp decline in precipitation after 3,700 cal. yr BP associated with an onset of a modern-style ENSO and characterised by increase in climatic variability. The decrease in precipitation and increased climate variability between 3,700 and 1,900 years ago would have resulted in reduced erosion and transport of sediment to the Gulf, and thus retard coastal progradation. Research by Moss et al. (2015) on Bentinck Island also identified that coastal wetland development occurred from ca. 2,400 to 500 years ago, consistent with a sea-level close to present levels and a hiatus in sediment supply to the coastal fringe.

Results indicate a more recent phase of dune formation and coastal progradation from 1,900 cal. yr BP (Figs 4 and 7). This is also consistent with palynological research on Bentinck Island showing an expansion of the mangrove fringe and the establishment of freshwater swamps in inter-dune swales (Moss et al., 2015). The increased sediment supply and recent phase of coastal dune building provided protection for expanding mangrove and freshwater swamps and most are likely associated with an increase in effective precipitation (Lees et al., 1990, Shulmeister and Lees, 1992).

The increased coastal dune and beach ridge activity from ca. 1900 years ago identified in this study and the region by Shulmeister and Lees (1992), Shulmeister (1999) and Nanson et al. (2013) is not restricted to northern Australia, but is a South Pacific-wide phenomenon. Research by Moy et al. (2002) from lacustrine deposits in Laguna Pallcacocha southern Ecuador also show a peak in ENSO amplitude occurring ca. 2,000 – 1,000 cal. yr BP, and then decreases towards modern times. Similarly, research in El Junco Crater Lake in the Galápagos Islands indicates increased precipitation and greatest ENSO variance in the Holocene occurred between 2,000±100 and 1,500±70 cal. yr BP (Conroy et al., 2008). When placed into a wider regional context results from this study show that coastal landscape evolution in the tropical north of Australia was not only dependent of sea-level change but also show a direct correlation with Holocene climate variability. Specifically, the formation and preservation of beach-rock deposits, intertidal successions, beach and chenier ridge systems hold valuable sea-level and Holocene climate proxies that can contribute to the growing research into lower latitude Holocene sea-level and climate histories.

6.4 Forcing functions for Holocene sea-level change

Rhodes (1982) and Chappell et al. (1982) attribute Holocene relative sea-level fall within the Gulf of Carpentaria to subsidence in northeastern Australia due hydro-isostatic loading. The subsidence in the central basin resulted in a forced regression due to uplift of between 0.2 – 1.4 m for the western Cape, and between 1.7 – 3.1 m in the Flinders-Leichhardt Region (Chappell et al. 1982; Fig. 1). However, Jones and Torgersen (1988) concluded that due to the continuous net accumulation of sediment on the Arafura Sill and within the central basin it is unlikely that significant uplift occurred, and the effects of subsidence would also have been minimal due to continuous lacustrine conditions during the last glacial phase. Results from this study also indicate that the influence of localized hydro-isostasy was minimal, and that eustatic sea-level change and equatorial syphoning were the driving force behind Holocene sea-level fluctuations.

The revised sea-level curve for the southern Gulf of Carpentaria is similar to sea-level histories from the east coast of Australia (Sloss et al., 2007, Woodroffe 2009, Lewis et al., 2013). For example, on the east coast of Queensland sea-level estimates based on coral microatolls and oyster beds indicate sea-level of between 1.3 to 1.6 m above PMSL between 6,770 and 5,700 cal. yr BP (Chappell et al., 1983; Beaman et al., 1994; Lewis et al., 2008, 2013; Yu and Zhao, 2010). Similar results were obtained by Horton et al. (2003, 2007) and Woodroffe et al. (2005) who analyzed intertidal foraminiferal to reconstruct former sea levels from mangrove environments from Cleveland Bay and the Great Barrier Reef. Their sea-level reconstruction shows an initial rapid rise during the early Holocene and a mid-Holocene highstand of ca. +1.7 above PMSL between 7,600 – 6,400 cal. yr BP.

On the southeast coast of Australia Sloss et al. (2005, 2007) also identified a rapidly rising sea-level following the LGM and a highstand of +1.5 m between 7,400 and 2,000 cal. yr BP. A full review of Holocene sea-level around the Australian continental margin is provided by Lewis et al. (2013) which shows that, in general, sea-level around the coastal margin of Australia attained PMSL between 8,000 and 7,400 cal. yr BP, with an elevation of between 1 and 2 m above PMSL, followed by a prolonged highstand until ca. 2,000 cal. yr BP.

The timing and elevation observed in the Gulf of Carpentaria as also similar to sea-level histories identified in the New Zealand Archipelago (Dougherty and Dickson, 2012; Clement et al., 2016). For example, the culmination of the most recent PMT occurred between 8,100 and 7,240 cal. yr BP and reached a maximum of 2.75 m above PMSL in the Northland region, and had fallen to present levels between 2,300 and 300 cal. yr. BP. In the South Island the culmination was slightly later, between 7,000 and 6,400 cal. yr. BP. The spatial and temporal variation in the timing and magnitude of Holocene sea-level in the New Zealand archipelago being regional differences in hydro-isostatic loading and continental tilting (Clement et al., 2016).

The similarities of the initial peak in sea-level during the most recent PMT observed in the Gulf of Carpentaria and other far-field sites indicates that eustatic sea-level due to melt-water influx during deglaciation resulted in regionally similar early Holocene sea-level history. The peak of sea-level during the culmination of the PMT observed in the Gulf of Carpentaria is also consistent with geophysical models that predict an initial first peak in sea-level between 7,000 and 6,800 cal. yr BP (Fleming et al., 1998; Lambeck, 2002; Peltier, 2002; Milne et al., 2005; Lambeck and Purcell, 2005).

However, the sea-level record from the Gulf of Carpentaria differs from those on the east coast of Australia, showing a shorter sea-level highstand and earlier regression to present levels from ca. 4,000 years ago. The short-lived highstand and fall of relative sea-level from ca. 4,000 years ago is consistent with geophysical models, and is also consistent with Holocene sea-level histories from other far-field sites that also show a regression over the past 4,000 years (Mitrovica and Milne, 2002). For example, evidence from emerged fossil reef platforms currently 1–3 m above PMSL in the South Pacific and Indian Ocean islands show that a 1 – 3 m fall in sea-level occurred over the last 6,500 years (Woodroffe and McLean 1990; Eisenhauer et al., 1999, 1993; Grossman et al., 1998; Banerjee, 2000; Woodroffe and Horton, 2005; Deschamps et al., 2012; Rashid et al., 2014). Horton et al. (2005) identified a sea-level fall following a 4,850–4,450 cal. yr BP Holocene highstand from the Great Songkhla Lakes and other areas on the Malaysia Peninsula. Mann et al. (2016) using fossil microatolls on reef flats on the Spermonde Shelf, Strait of Makassar, also identified a sea-level highstand of <0.5 m above PMSL ca. 5,600 cal. yr BP. The highstand was followed by a relatively rapid sea-level fall towards present sea levels from ca. 4,000 cal. yr BP. Rashid et al. (2014) also identified a sea-level fall of 2 m following the Holocene maximum at 4,500 cal. yr BP around the Society Islands in French Polynesia. However, Holocene sea-level reconstructions from far-field sites cover a large geographical region and show a great deal of variability in the timing and magnitude and duration of the mid-Holocene highstand due to regional and local neo-tectonics and hydro-isostatic influences. Nevertheless, the nature of Holocene sea-level change is broadly similar (Woodroffe and Horton, 2005; Horton, 2006; Lewis et al., 2013).

The difference between the prolonged highstand observed along the eastern sea-board of Australia versus the short highstand observed in the Gulf of Carpentaria and other far-field sites raises the question of variability in mid-to-late Holocene sea-level records. The driving force behind the difference is hypothesized here to be a greater influence of equatorial ocean siphoning where water is drawn from the lower latitude equatorial oceans to fill accommodation caused by the collapsing peripheral forebulge around formerly glaciated regions (Woodroffe and McLean, 1990; Milne and Mitrovica, 1998; Mitrovica and Milne, 2002). It is hypothesized that higher latitudes in far-field sites (e.g. east coast of Australia and North Island of New Zealand) were influenced by the relocation of equatorial waters and a prolonged melt-water input from Antarctica (Goodwin, 1998, 2003). Ocean syphoning to higher latitudes would result in a relative sea-level fall in lower latitudes and an extended Holocene sea-level highstand in higher latitudes in far-field sites until ca. 2,000 cal. yr BP. The extended highstand around much of the continental margin of Australia does not fit well with existing geophysical models for far-field sites (Fleming et al., 1998; Lambeck, 2002; Peltier, 2002; Milne et al., 2005). For example, geophysical models presented by Chappell et al. (1982) and Lambeck and Nakada (1990) predict a smooth sea-level fall following the initial peak in sea-level for the far-field sites, suggesting negligible contribution from ice melting after 7,000 – 6,000 cal. yr BP. However, several authors are now promoting an extended Holocene highstand based on empirical data that represents a gradual, rather than abrupt, end to global ice melt, continuing into the late Holocene (Goodwin 1998, 2003; Woodroffe et al., 2005, Woodroffe and Horton, 2005; Sloss et al., 2007; Lewis et al., 2013). The combined effects of equatorial syphoning and prolonged melt-water input from Antarctica explain the short highstand in the tropical north of Australia and the extended highstand in higher latitudes around the Australian continental margin.

7 Conclusions

The compilation of results from previous research, and results of this research, indicate that rising sea levels beached the Arafura Sill ca. 11,700 cal. yr BP, with full marine conditions being attained in the Gulf of Carpentaria by 10,500 cal. yr BP. Inundation resulted in coral reef development between 10,500 and 9,500 cal. yr BP at elevations between 20 and 30 m below PMSL. Sea-level continued to rise to attained PMSL ca. 7,700 cal. yr BP and attained a highstand of between +1.5 and +2 m by ca. 7,000 cal. yr BP. Sea-level highstand remained between +1.5 and +2 m above PMSL until ca. 4,000 cal. yr BP, followed by a fall to near present.

This sea-level history has significantly influenced coastal landscape evolution. The culmination of the most recent PMT and Holocene sea-level highstand (7,700 – 4,000 years ago) saw the deposition and formation of beach-rock facilitated by a positive sediment budget to the nearshore associated with rapidly rising sea levels, as well as a period of increased precipitation and temperature during the Holocene climate optimum. During this phase, transgressive deposits, the formation of mangrove fringe around the islands, and the initiation of the first phase of dune and chenier ridge development occurred. Coastal progradation of coastal beach and chenier ridges occurred following decrease in accommodation space associated with a rapid fall in sea-level between 4,000 and 3,700 years ago, and again from 1900 years ago to the present, strongly influenced by climate variability associated with the intensification of the ENSO.

The sea-level history observed in the southern Gulf of Carpentaria calls into question the role of localized hydro-isostasy on relative sea-level history in the region, and provides additional data for ongoing research into the Holocene eustatic sea-level change and the influence of ocean syphoning during the mid-to-late Holocene. When placed into context with other far-field sites, results from the Gulf of Carpentaria indicate that there is a significant latitudinal difference associated with Holocene sea-level histories in far-field sites. Lower latitude sites commonly display a sea-level history consistent with geophysical models and are characterised by short-lived highstand and fall in relative sea-level from ca. 4,000 years ago. The driving force is hypothesized to be a cessation of melt-water input following the culmination of the most recent PMT, and equatorial syphoning. Higher latitude far field sites commonly show a more extended Holocene sea-level highstand to ca. 2,000 years ago before falling to present levels. The extended sea-level highstand hypothesized to be a continuing (but reduced) melt-water input over the mid-Holocene, and contributions from lower latitudes due to ocean syphoning. However, the precise transition between sea-level histories in far-field sites is yet to be determined and is complicated by regional hydro-isostatic and neo-tectonic activity. Results from this research provide a detailed regional sea-level curve for northern Australia, quantified the influence of Holocene sea-level fluctuations on coastal landscape evolution, and contribute to ongoing research into the nature and driving mechanisms for mid-to-late Holocene sea-level change. This research also highlights the need for additional detailed regional and even local-scale sea-level histories to quantify the influence of equatorial syphoning, hydro-isostatic and neo-tectonic activity on sea-level histories in far field sites.

Acknowledgements

This project was supported under the Australian Research Council's Discovery Projects (project numbers DP120103179 and DP0663047) and Australian Institute of Nuclear Sciences and Engineering (ALNGRA13017, ALNGRA15513) funding schemes. SU is the recipient of an Australian Research Council Future Fellowship (FT120100656). We acknowledge the financial support from the Australian Government for the Centre for Accelerator Science at ANSTO through the National Collaborative Research Infrastructure Strategy (NCRIS). We acknowledge Kaiadilt traditional owners of the South Wellesley Islands as partners in this research. The Kaiadilt Aboriginal Corporation collaborated in establishing the research framework for this project. We extend a special thanks to Duncan Kelly and Lincoln Steinberger for assistance in the field. Thanks go to Tex and Lyn Battle for assistance with logistics. This paper is a contribution to the International Quaternary Association (INQUA) working group on “Coastal and Marine Processes” and SHAPE (Southern Hemisphere assessment of palaeoenvironments).

Reference List

Augustinus, P. G. E. F., 1989. Cheniers and chenier plains: a general introduction. *Marine Geology*,90, 219–229.

Augustinus, P. G. E. F., Hazelhoff, L., Kroon, A., 1989. The chenier coast of Suriname: modern and geological development. *Marine Geology* 90, 269–281.

Baker, R. G. V., Haworth, R. J., 1997. Further evidence fromrelic shellcrust sequences for a late Holocene higher sea level for eastern Australia. *Marine Geology* 141, 1-9.

Baker, R.G.V., Haworth, R.J., 2000a. Smooth or oscillating late Holocene sea-level curve? Evidence from the palaeo-zoology of fixed biological indicators in east Australia and beyond. *Marine Geology* 163, 367-386.

Baker, R.G.V., Haworth, R.J., 2000b. Smooth or oscillating late Holocene sea-level curve? Evidence from cross-regional statistical regressions of fixed biological indicators. *Marine Geology* 163, 353-365.

Baker, R.G.V., Haworth, R.J., Flood, P.G., 2001a. Warmer or cooler late Holocene marine palaeoenvironments?: interpreting southeast Australian and Brazilian sea-level changes using fixed biological indicators and their d18O composition. *Palaeogeography, Palaeoclimatology, Palaeoecology* 168, 249-272.

Baker, R.G.V., Haworth, R.J., Flood, P.G., 2001b. Inter-tidal fixed indicators of former Holocene sea levels in Australia: a summary of sites and a review of methods and models. *Quaternary International* 83-85, 257-273.

Baker, R.G.V., Haworth, R.J., Flood, P.G., 2005. An oscillating Holocene sea-level? Revisiting Rottnest Island, Western Australia, and the Fairbridge eustatic hypothesis. *Journal of Coastal Research, Special Issue* 42, 3-14.

Banerjee, P. K., 2000. Holocene and Late Pleistocene relative sea level fluctuations along the east coast of India. *Marine Geology* 167, 243-260.

Beaman, R., Larcombe, P., Carter, R. M., 1994. New evidence for the Holocene sea level high from inner shelf central Great Barrier Reef, Australia. *Journal of Sedimentary Research* A64, 881-885.

Benac, C., Juracic, M., Bakran-Petricioli, T., 2004. Submerged tidal notches in the Rijeka Bay NE Adriatic Sea: indicators of relative sea-level change and of recent tectonic movements. *Marine Geology* 212, 21–33.

Bronk Ramsey, C., 2009. Bayesian analysis of radiocarbon dates. *Radiocarbon* 51, 337-360.

Brooke, B., Lee, R., Cox, M., Olley, J., Pietsch, T., 2008. Rates of shoreline progradation during the last 1700 years at Beachmere, southeastern Queensland, Australia, based on optically stimulated luminescence dating of beach ridges. *Journal of Coastal Research* 24 (3), 640-648.

Brooke, B.P., Nichol, S. L., Huang, Z., Beaman, R., 2017, Palaeoshorelines on the Australian continental shelf: Morphology, sea-level relationship and applications to environmental management and archaeology. *Continental Shelf Research* 134, 26–38.

Bureau of Meteorology (BOM) 2016 *Monthly Climatic Statistics for Sweers Island, Queensland*. Retrieved 29/04/2016 from <http://www.bom.gov.au/climate/averages/tables/cw_029139.shtml>.

Carpenter, K.E.; Niem, V.H. (eds). 1998. FAO species identification guide for fishery purposes. The living marine resources of the Western Central Pacific. Volume 1. Seaweeds, corals, bivalves and gastropods. Rome, FAO, pp. 1-686.

Clark, T. R., Zhao, J.-x., Feng, Y.-x., Done, T. J., Jupiter, S., Lough, J., Pandolfi, J. M. 2012. Spatial variability of initial 230Th/232Th in modern Porites from the inshore region of the Great Barrier Reef. *Geochimica et Cosmochimica Acta* 78, 99-118.

Clement, A. J. H., Whitehouse P. L., Sloss, C. R. 2016. An examination of spatial variability in the timing and magnitude of Holocene relative sea-level changes in the New Zealand archipelago. *Quaternary Science Reviews* 131, 73 – 101.

Chappell, J., Chivas, A., Wallensky, E., Polach, H.A., Aharon, P., 1983. Holocene palaeo-environmental changes, central to north Barrier Reef inner zone. *BMR Journal of Australian Geology and Geophysics*, 8, 223-235.

Chappell, J., Rhodes, E.G., Thom, B. G., Wallensky, E., 1982. Hydro-isostasy and the sea-level isobase of 5500 B.P. in North Queensland, Australia. *Marine Geology* 49, 81-90.

Chappell, J., Thom, B. 1986. Coastal morphodynamics in North Australia: review and prospect. *Australian Geographical Studies* 24(1), 110-127.

Chivas, A.R., Garcia, A., van der Kaars, S., Couapel, M.J.J., Holt, S., Reeves, J.M., Wheeler,D.J., Switzer, A.D., Murray- Wallace, C.V., Banerjee, D., Price, D.M., Wang, S.X., Pearson, G., Edgar, N.T., Beaufort, L., De Deckker, P., Lawson, E.M., Cecil, C.B., 2001. Sea-level and environmental changes since the last interglacial in the Gulf of Carpentaria, Australia: an overview. *Quaternary International* 83-85, 19-46.

Church, J. A, Forbes, A. M. G. 1981. Non-linear model of the tides in the Gulf of Carpentaria. *Australian Journal of Marine and Freshwater Research* 32, 685-697.

Conroy, J. L., Overpeck, J. T., Cole, E., Shanahan, T. M., Steinitz-Kannan, M., 2008. Holocene changes in eastern tropical Pacific climate inferred from a Galápagos lake sediment record. *Quaternary Science Reviews* 27, 1166–1180.

Day, R. W. 1983. *Queensland Geology: A companion volume to the 1: 2,500,000 scale geological map (1975)*. Geological Survey of Queensland.

Deschamps, P., Durand, N., Bard, E., Hamelin, B., Camoin, G., Thomas, A. L., Henderson, G. M., Okuno, J., Yokoyama, Y., 2012. Ice-sheet collapse and sea-level rise at the Bølling warming 14,600 years ago. *Nature* 483, 559-564.

Desruelles, S., Fouache, E., Ciner, A., Dalongeville, R., Pavlopoulos, K., Kosun, E., Coquinot, Y., Potdevin, J.L., 2009. Beach-rocks and sea level changes since Middle Holocene: comparison between the insular group of Mykonos-Delos-Rhenia (Cyclades, Greece) and the southern coast of Turkey. *Global and Planetary Change* 66, 19-33.

Dougherty, A. J., Dickson, M. E. 2012. Sea level and storm control on the evolution of a chenier plain, Firth of Thames, New Zealand. *Marine Geology* 307-310, 58-72.

Eisenhauer, A., Wasserburg, G. J., Chen, J. H., Bonani, G., Collins, L. B., Zhu, Z. R., Wyrwoll, K. H., 1993. Holocene sea-level determination relative to the Australian continent: U/Th (TIMS) and 14C (AMS) dating of coral cores from the Abrolhos Islands. *Earth and Planetary Science Letters* 114, 529-547.

Eisenhauer, A., Heiss, G. A., Sheppard, C., Dullo, W. C., 1999. Reef and island formation and Late Holocene sea level changes in the Chagos islands. In: Sheppard, C.R.C., Seaward, M.R.D. (Eds.), Ecology of the Chagos Archipelago. Westbury Publishing, Otley, 350 pp.

Engelhart, S. E., Horton, B. P., Douglas, B. C., Peltier, W.R., Törnqvist, T. E. 2009. Spatial variability of late Holocene and 20th century sea-level rise along the Atlantic coast of the United States. *Geology* 37, 1115-1118.

Fink, D., Hotchkis, M., Hua, Q., Jacobsen, G., Smith, A.M., Zoppi, U., Child, D., Mifsud, C., van der Gaast, H., Williams, A., Williams, M., 2004. The ANTARES AMS facility at ANSTO. Nucl. Instrum. Methods Phys. Res. B 223-224, 109-115.

Fleming, K., Johnston, P., Zwartz, D., Yokoyama, Y., Lambeck, K., Chappell, J., 1998. Refining the eustatic sea-level curve since the Last Glacial Maximum using far- and intermediate-field sites. *Earth and Planetary Science Letters* 163 (1-4), 327-342.

Geocentric Datum of Australia: Technical Manual. Intergovernmental Committee on Surveying and Mapping (ICSM) and Permanent Committee on Geodesy (PCG).

Goodwin, I. D., 1998. Did changes in Antarctic ice volume influence late Holocene sea-level lowering? *Quaternary Science Reviews* 17, 319-332.

Goodwin, I. D., 2003. Unravelling climatic influences on Late Holocene sea-level variability. In: Mackay, A., Battarbee, R., Birks, J., Oldfield, F. (Eds.), Global Change in the Holocene. Hodder Arnold, pp. 406-421.

Grimes, K. G. 1979. *Mornington - Cape Van Diemen, Queensland: sheet SE/54-1/2 international index*. Australian Government Publishing Service.

Grindrod, J., Rhodes, E. G., 1984. Holocene sea-level history of a tropical estuary: Missionary Bay, north Queensland. In: Thom, B. G. (Ed.), Coastal Geomorphology in Australia. Academic Press, Australia, pp. 151-178.

Grindrod, J., Moss, P., van der Kaars, S., 1999. Late Quaternary cycles of mangrove development and decline on the north Australian continental shelf. *Journal of Quaternary Science* 14, 465-470.

Grindrod, J, Moss, P.T. and van der Kaars, S., 2002. Late Quaternary mangrove pollen records from the continental shelf and deep ocean cores in the north Australian region. In (Eds). Kershaw, A.P., David, B., Tapper, T., Penny, D. and Brown, J. *Bridging Wallace's Lines – The Environmental and Cultural History and Dynamics of the SE-Asian-Australian Region*). *Advances in Geoecology 34,* Cantena Verl., Reiskirchen, Germany pp. 119 to 148.

Grossman, E. E., Fletcher III, C. H., Richmond, B. M. 1998. The Holocene sea-level highstand in the equatorial Pacific: analysis of the insular paleosea-level database. *Coral Reefs* 17 (3), 309-327.

Harris, P.T., Heap, A., Marshall, J.F., Hemer, M., Daniell, J., Hancock, A., Buchanan, C., Sbaffi, L., Brewer, D., Heales, D., 2007. Submerged coral reefs and benthic habitats of the southern Gulf of Carpentaria. Geoscience Australia Record, 2007/02: 134.

Harris, P.T., Heap, A.D., Marshall, J.F., McCulloch, M., 2008. A new coral reef province in the Gulf of Carpentaria, Australia: Colonisation, growth and submergence during the early Holocene. *Marine Geology* 251, 85-97.

Hearty, P, J., Hollin, J. T., Conrad Neumann, A., O'Leary, M. J., McCulloch, M., 2007. Global sea-level fluctuations during the Last Interglaciation (MIS 5e). *Quaternary Science Reviews* 26 (17-18), 2090–2112.

Hendry, M., Digerfeldt, G., 1989. Palaeogeography and palaeoenvironments of a tropical coastal wetland and offshore shelf during Holocene submergence, Jamaica. *Palaeogeography, Palaeoclimatology, Palaeoecology* 73 (1-2), 1-10.

Hodgson, G. M., 1998. Corals. In: Carpenter, K.E.; Niem, V.H. (eds). FAO species identification guide for fishery purposes. The living marine resources of the Western Central Pacific. Volume 1. Seaweeds, corals, bivalves and gastropods. Rome, FAO, pp. 1-686.

Hopley, D., 1986. Beach-rock as a sea-level indicator. In Van de Plassche, O. (ed.), Sea-level Research: A Manual for the Collection and Evaluation of Data. Norwich: Geo Books, pp. 157–173.

Hopley, D., Smithers, S. G., Parnell, K., 2007. Geomorphology of the Great Barrier Reef: Development, Diversity and Change. Cambridge University Press, 546 pp.

Horton, B. P., 2006. Late Quaternary Relative Sea-level Changes in Mid-latitudes. In: Elias, S. A (Ed) Encyclopedia of Quaternary Science. Boston, Elsevier, Boston, USA, pages 2064-3071.

Horton, B.P., Larcombe, P., Woodroffe, S.A., Whittaker, J. E., Wright, M. R., Wynn, C., 2003. Contemporary foraminiferal distributions of a mangrove environment, Great Barrier Reef coastline, Australia: implications for sea-level reconstructions. *Marine Geology* 198, 225-243.

Horton, B. P., Gibbard, P. L., Milne, G. M., Morley, R. J., Purintavaragul, C., Stargardt, J. M., 2005. Holocene sea levels and palaeoenvironments, Malay-ai Peninsula, southeast Asia. *The Holocene*, 15 (8), 1199-1213.

Horton, B. P., Culver, S. J., Hardbattle, M. I. J., Larcombe, P., Milne, G. A., Morigi, C., Whittaker, J. E., Woodroffe, S. A., 2007. Reconstructing Holocene sea-level change for the central Great Barrier Reef (Australia) using subtidal foraminifera. *Journal of Foraminiferal Research* 37, 327-343.

Hua, Q., Jacobsen, G.E., Zoppi, U., Lawson, E.M., Williams, A.A., Smith, A.M., McGann, M.J., 2001. Progress in radiocarbon target preparation at the ANTARES AMS Centre. Radiocarbon 43, 275-282.

Jones, M.R., Torgersen, T., 1988. Late Quaternary evolution of Lake Carpentaria on the Australian-New Guinea continental shelf. *Australian Journal of Earth Sciences*, 35, 313-324.

Jones, B.G., Young, R.W., Eliot, I.G., 1979. Stratigraphy and chronology of receding barrier beach deposits on the northern Illawarra coast of New South Wales. *Journal of the Geological Society of Australia* 26, 255-264.

Kershaw, S., Guo, L., 2001. Marine notches in coastal cliffs: indicators of relative sea-level change, Perachora Peninsula, central Greece. *Marine Geology*, 179, 213-228.

Komar, P. D., 1998. Beach Processes and Sedimentation. 2nd ed. Upper Saddle River, New Jersey: Prentice Hall.

Lambeck, K., 2002. Sea level change from Mid Holocene to Recent time: An Australian example with global implications. In: Mitrovica, J.X., Vermeersen, B. (Eds.), Ice Sheets, Sea Level and the Dynamic Earth, Vol. 29. AGU, pp. 33-50.

Lambeck, K., Nakada, M., 1990. Late Pleistocene and Holocene sea-level change along the Australian coast. *Palaeogeography, Palaeoclimatology, Palaeoecology*, 89, 143-176.

Lambeck, K., Purcell, A., 2005. Sea-level change in the Mediterranean Sea since the LGM: model predictions for tectonically stable areas. *Quaternary Science Reviews* 24, 1969-1988.

Lees, B. G., 1987. Age structure of the Point Stuart chenier plain: a reassessment. *Search*, 18, 257-259.

Lees, B. G., Lu, Y., Head, J., 1990. Reconnaissance thermoluminescence dating of northern Australian coastal dunefields. *Quaternary Research* 34, 169-185.

Leonard, N. D., Welsh, K. J., Zhao, J.-x., Nothdurft, L. D., Webb, G. E., Major, J., Feng, Y., Price, G. J. 2013. Mid-Holocene sea level and coral reef demise: U-Th dating of subfossil corals in Moreton Bay, Australia. *The Holocene* 23 (12), 1841-1852.

Lewis, S.E., Wüst, R.A.J., Webster, J.M., Shields, G.A., 2008. Mid-late Holocene sea level variability in eastern Australia. *Terra Nova* 20, 74 - 81.

Lewis, S., E., Sloss, C. R., Murray-Wallace, C. V., Woodroffe, C. D., Smithers, S. G., 2013. Post- glacial sea-level changes around the Australian margin: A review. *Quaternary Science Reviews* 74, 115 – 138.

Lewis, S. E., Wüst, R. A. J., Webster, J. M., Collins, J., Wright, S. A., Jacobsen, G. 2015. Rapid relative sea-level fall along north-eastern Australia between 1200 and 800 cal. yr BP: An appraisal of the oyster evidence. *Marine Geology* 370, 20-30.

Mackenzie, L., 2016. Palaeoecology of the South Wellesley Archipelago. A history of human occupation and environmental change. PhD Thesis, School of Geography, Planning and Environmental Management, The University of Queensland.

Mann, T., Rovere, A., Scone, T., Klicpera, A., Stocchi, P., Muhammad, L., Westphal, H., 2016. The magnitude of a mid-Holocene sea-level highstand in the Strait of Makassar. *Geomorphology* 257, 155 – 163.

McBride, R. A., Taylor, M. T. and Byrnes, M. R., 2007. Coastal morphodynamics and Chenier-Plain evolution in southwestern Louisiana, USA: A geomorphic model. *Geomorphology* 88, 367–422.

McLean, R. F., 2011. . In Hopley, D., (ed.), Encyclopedia of Modern Coral Reefs, edn. Original, Springer, The Netherlands, pp.107-111.

Memmott, P., Round, E., Rosendahl, D., Ulm, S., 2016. Fission, fusion and syncretism: linguistic and environmental changes amongst the Tangkic people of the southern Gulf of Carpentaria, northern Australia. In: Verstraete, J-C., Hafner, D., (eds), *Land and Language in Cape York Peninsula and the Gulf Country*, pp. 105-136 (John Benjamins Publishing Company, Amsterdam).

Milne, G. A., Mitrovica, J. X., 1998. Postglacial sea-level change on a rotating Earth. *Geophysical Journal International* 133, 1–19.

Milne, G. A., Long, A. J., Bassett, S. E., 2005. Modelling Holocene relative sea-level observations from the Caribbean and South America. *Quaternary Science Reviews* 24, 1183-1202.

Mitrovica, J. X., Milne, G. A., 2002. On the origin of late Holocene sea-level highstands within equatorial ocean basins. *Quaternary Science Reviews* 21, 2179–2190.

Moss, P. T., Mackenzie, L., Ulm, S., Sloss, C. R., Rosendahl, D. E., Petherick, L. M., Steinberger, L. M., Wallis, L., Heijnis, H., Petchey, F., Jacobsen, G., 2015. Environmental Context for Late Holocene Human Occupation of the South Wellesley Archipelago, Gulf of Carpentaria, Northern Australia. *Quaternary International* 385, 136-144.

Moy, C. M., Seltzer, G. O., Rodbell, D. T., Anderson, D. M., 2002. Variability of El Niño/Southern Oscillation activity at millennial timescales during the Holocene epoch. *Nature* 420 (6912), 162-165.

Nanson, R. A., Vakarelov, B. K., Ainsworth, R. B., Williams, F. M., Price, D. M., 2013. Evolution of a Holocene, mixed-process, forced regressive shoreline: the Mitchell River delta, Queensland, Australia. *Marine Geology* 339, 22-43

Neumann, A. C., Hearty, P. J., 1996. Rapid sea-level changes at the close of the Last Interglacial (stage 5e) recorded in Bahamian Island geology. *Geology* 24, 775–778.

Nott, J., Goff, J., Change-Goff, C., Sloss, C., Riggs, N., 2013. Anatomy of sand beach ridges: evidence from severe Tropical Cyclone Yasi and its predecessors, northeast Queensland, Australia. *Journal of Geophysical Research: Earth Surface* 118, 1–10.

Nott, J., 1996. Late Pleistocene and Holocene Sea-Level Highstands in Northern Australia. *Journal of Coastal Research* 12, 907-910.

Otvos, E. G., 2000. Beach ridges – Definitions and significance. *Geomorphology* 32, 83-108.

Otvos, E.G., 2004. Holocene sea-levels: recognition issues and an updated sea-level curve. *Journal of Coastal Research* 20,

Otvos, E.G., 2005. Validity of sea-level indicators: A comment on A new depositional model for the buried 4000 yr BP New Orleans barrier: implications for sea-level fluctuations and onshore transport from a nearshore shelf source by F.W. Stapor and G.W. Stone [Marine Geology 204 (2004) 215–234]680– 699. *Marine Geology* 217, 177-187.

Parkinson, R. W., 1989. Decelerating Holocene sea-level rise and its influence on Southwest Florida coastal evolution: A transgressive/regressive stratigraphy. *Journal of Sedimentary Petrology* 59 (6), 960-972.

Peltier, W. R., 2002. On eustatic sea level history: Last Glacial Maximum to Holocene. *Quaternary Science Reviews* 21, 377-396.

Pirazzoli, P. A., 1986. Marine notches. In: van de Plassche, O. (Ed.). Sea-level Research: A Manual for the Collection and Evaluation of Data. Geo Books, Norwich, UK, pp. 361-400.

Pirazzoli, P. A., 1996. Sea-level Changes: The Last 20,000 Years. John Wiley & Sons, West Sussex, England.

Rashid, R., Eisenhauer, A., Stocchi, P., Liebetrau, V., Fietzke, J., Rüggeberg, A., Dullo, W-C., 2014. Constraining mid to late Holocene relative sea level change in the southern equatorial Pacific Ocean relative to the Society Islands, French Polynesia. *Geochemistry, Geophysics, Geosystems* 15, 2601–2615.

Reeves, J.M., Barrows, T.T., Cohen, T.J., Kiem, A.S., Bostock, H.C., Fitzsimmons, K., Jansen, J.D., Kemp, J., Krause, C., Petherick, L., Phipps, S. and OZ-INTIMATE members, 2013. Climate variability over the last 35,000 years recorded in marine and terrestrial archives in the Australian region: an OZ-INTIMATE compilation. *Quaternary Science Reviews* 74: 21-34.

Reeves, J.M., A.R. Chivas, A. Garcia and P. De Deckker 2007 Palaeoenvironmental change in the Gulf of Carpentaria (Australia) since the last interglacial based on Ostracoda. *Palaeogeography, Palaeoclimatology, Palaeoecology* 246:163-187.

Reeves, J.M., Chivas, A.R., Garcia, A., Holt, S., Couapel, M.J.J., Jones, B., Cendon, D.I., Fink, D., 2008. The sedimentary record of palaeoenvironments and sea-level change in the Gulf of Carpentaria, Australia, through the last glacial cycle. *Quaternary International* 183, 3-

Reimer, P.J., Bard, E., Bayliss, A., Beck, J.W., Blackwell, P.G., Bronk Ramsey, C., Buck, C.E., Cheng, H., Edwards, R.L., Friedrich, M., Grootes, P.M., Guilderson, T.P., Hafl-idason, H., Hajdas, I., Hatte, C., Heaton, T.J., Hoffmann, D.L., Hogg, A.G., Hughen, K.A., Kaiser, K.F., Kromer, B., Manning, S.W., Niu, M., Reimer, R.W., Richards, D.A., Scott, E.M., Southon, J.R., Staff, R.A., Turney, C.S.M., van der Plicht, J., 2013. IntCal13 and Marine13 radiocarbon age calibration curves 0-50,000 years cal BP. Radiocarbon 55, 1869-1887.

Rhodes, E. G., 1982. Depositional model for a chenier plain, Gulf of Carpentaria, Australia *Sedimentology* 29, 201-221.

Rhodes, E. G., Polach, H. A., Thom, B. G., Wilson, S. R., 1980. Age structure of Holocene coastal sediments: Gulf of Carpentaria, Australia. *Radiocarbon*, 22, 718 – 727.

Rosendahl, D., 2012. The Way it Changes Like the Shoreline and the Sea: The Archaeology of the Sandalwood River, Mornington Island, Southeast Gulf of Carpentaria, Australia. A Thesis submitted for the Degree of Doctor of Philosophy at the University of Queensland.

Rosendahl, D., Lowe, K. M., Wallis, L. A., Sean Ulm, S., 2014. Integrating geoarchaeology and magnetic susceptibility at three shell mounds: a pilot study from Mornington Island, Gulf of Carpentaria. *Australia Journal of Archaeological Science* 49, 21-32

Rosendahl, D. E., Ulm, S., Sloss, C. R., Steinberger, L. M., Petchey, F., Jacobsen, G., Stock, E., Robins, R., 2015. Mid-Holocene Aboriginal Occupation of Offshore Islands in Northern Australia? A Reassessment of Wurdukanhan, Mornington Island, Southern Gulf of Carpentaria, Australia. *Quaternary International* 385, 145-153.

Rovere, A., Stocchi, P., Vacchi, M. 2016. Eustatic and relative sea level changes. *Current Climate Change Reports*, 2(4):221-231.

Saenger, P. 2005 Sweers Island: Changes over two hundred years since Flinders' visit. In J.W. Johnson and A.C. Gill (eds), Gulf of Carpentaria Scientific Study Report, pp.1-23. Geography Monograph Series 10. Brisbane: Royal Geographic Society of Queensland.

Saenger, P., Hopkins, M. S. 1975. Observations on the mangroves of the south-eastern Gulf of Carpentaria, Australia. *First Intern. Symp. Biology & Management of Mangroves, University of Florida*, 1, 126–136.

Saito, Y., Wei, H., Zhou, Y., Nishimura, A., Sato, Y., Yokota, S., 2000. Delta progradation and chenier formation in the Huanghe (Yellow River) delta, China. *Journal of Asian Earth Sciences* 18, 489–497.

Saito, Y., Yang, Z. S., hori, K. 2001. The Huanghe (Yellow River) and Changjiang (Yangtze River) deltas: a review on their characteristics, evolution and sediment discharge during the Holocene. *Geomorphology* 41, 219-231.

Scheffers, A., Engel, M., Scheffers, S., Squire, P., Kelletat, D., 2011. Beach ridge systems – archives for Holocene coastal events? *Progress in Physical Geography* 36, 5–37.

Shennan, I., Horton, B., 2002. Holocene land- and sea-level changes in Great Britain. *Journal of Quaternary Science* 17, 511-526.

Scholl, D. W., 1964. Recent sedimentary record in mangrove swamps and rise in sea level over the southwestern coast of Florida: Part 1. *Marine Geology* 1, 344-366.

Scholl, D. W., Craighead Jr., F. C., Stuiver. M., 1969. Florida submergence curve revised: Its relation to coastal sedimentation rates. *Science*, 163, 562-564.

Shulmeister, J., 1999. Australasian evidence for mid-Holocene climate change implies precessional control of Walker Circulation in the Pacific. *Quaternary International*, 57-58, 81-91.

Shulmeister, J., Lees, B. G., 1992. Morphology and chronostratigraphy of a coastal dunefield; Groote Eylandt, northern Australia. *Geomorphology*, 5 (6), 521-534.

Sloss, C. R., Jones, B. G., Murray-Wallace, C. V., McClennen, C. E. 2005 Holocene sea level fluctuations and the sedimentary evolution of a barrier estuary: Lake Illawarra, New South Wales, Australia. *Journal of Coastal Research* 21(5):943-959.

Sloss, C.R., Murray-Wallace, C.V., Jones, B.G., 2007. Holocene sea-level change on the southeast coast of Australia: a review. *The Holocene* 17, 999-1014.

Sloss, C. R., Jones, B. G., Brooke, B. P., Heijnis, H., Murray-Wallace, C. V., 2011. Contrasting sedimentation rates in Lake Illawarra and St Georges Basin, two large barrier estuaries on the southeast coast of Australia. *Journal of Paleolimnology*, 46, 561-577.

Sloss, C. R., Westaway, K., Hau, Q., Murray-Wallace, C. V., 2013. Chapter: 14.36 An introduction to dating techniques: A guide for Geomorphologists. In: John F. Shroder, (Ed) Treatise on Geomorphology, Vol. 14: Methods in Geomorphology, Elsevier, Academic Press, San Diego, p. 119-137.

Smart, J., Grimes, K., Doutch, H., Pinchin, J. 1980. *The Mesozoic Carpentaria Basin and the Cainozoic Karumba Basin, North Queensland*. Australian Government Pub. Service.

Smithers, S., 2011. Sea-level indicators. In Hopley, D., (ed.) Encyclopedia of Modern Coral Reefs: structure, form and process. Encyclopedia of Earth Science . Springer, Dordrecht, The Netherlands, pp. 978-991.

Stattegger, K., Tjallingii, R., Saito, Y., Michelli, M., Than, N. T., Wetzel, A., 2013. Mid to Late Holocene sea-level reconstruction of Southeast Vietnam using beach-rock and beach- ridge deposits. *Global and Planetary Change*, 110(B), 214-222.

Tamur, Y., 2012. Beach ridges and prograded beach deposits as palaeoenvironment records *Earth-Science Reviews*, 114, 279–297.

Tanner, W. F., 1995. Origin of beach ridges and swales. *Marine Geology* 129, 149-161.

Tanner, W. F., 1988. Beach-ridge data and sea-level history from the Americas. *Journal of Coastal Research*, 4 (1), 81-91.

Taylor, M. J., Stone, G. W., 1996. Beach-ridges: A review. *Journal of Coastal Research* 12, 612-621.

Thom, B.G., Roy, P., 1983. Sea level change in New South Wales over the past 15000 years. In: Hopley, D. (Ed.), Australian Sea Levels in the last 15000 Years: a Review. Monograph Series Occasional Paper 3. Geography Department, James Cook University, Townsville, pp. 64-84.

Thom, B.G., Roy, P., 1985. Relative sea levels and coastal sedimentation in southeast Australia in the Holocene. *Journal of Sedimentary Petrology*, 55, 257-264.

Torgersen, T., M.F. Hutchinson, D.E. Searle and H.A. Nix 1983 General bathymetry of the Gulf of Carpentaria and the Quaternary physiography of Lake Carpentaria. *Palaeogeography, Palaeoclimatology, Palaeoecology* 41(3-4):207-225.

Torgersen, T., J. Luly, P. De Deckker, M.R. Jones, D.E. Searle, A.R. Chivas and W.J. Ullman 1988 Late Quaternary environments of the Carpentaria Basin, Australia. *Palaeogeography, Palaeoclimatology, Palaeoecology* 67(3-4):245-261.

Ulm, S., 2006. Australian marine reservoir effects: A guide to □R values. *Australian Archaeology*, 63, 57-60.

Ulm, S., Evans, N., Rosendahl, D., Memmott, P., Petchey, F., 2010. Radiocarbon and linguistic dates for occupation of the south Wellesley Islands, northern Australia. *Archaeology in Oceania* 45 (1), 39-43.

Umitsu, M., Buman, M., Kawase, K., Woodroffe, C. D. 2001. Holocene palaeoecology and formation of the Shoalhaven River deltaic-estuarine plains, southeast Australia. *The Holocene* 11, 407-418.

Vousdoukas, M. I., Velegrakis, A. F., Plotmaritis, T. A., 2007. Beach-rock occurrence, characteristics, formation mechanisms and impacts. *Earth-Science Reviews*, 85, 23-46.

Wang, H., van Strydonck, M., 1997 Chronology of Holocene cheniers and oyster reefs on the coast of Bohai Bay, China. *Quaternary Research*, 47, 192-205.

Weill, P., Tessier, B., Mouazé, D., Bonnot-Courtois, C., Norgeot, C., 2012. Shelly cheniers on a modern macrotidal flat (Mont-Saint-Michel bay, France) — Internal architecture revealed by ground-penetrating radar. *Sedimentary Geology*, 279, 173–186.

Wolanski, E. 1993 Water circulation in the Gulf of Carpentaria. *Journal of Marine Systems* 4:401-420.

Woodroffe, C. D., 1981. Mangrove swamp stratigraphy and Holocene transgression, Grand Cayman Island, West Indies. *Marine Geol*ogy 41, 271-294.

Woodroffe, C.D., 1988. Mangroves and sedimentation in reef environments: indicators of past sea-level changes, and present sea-level trends? Proceedings of the Sixth International Coral Reef Symposium, Australia, 3, 535-539.

Woodroffe, C.D., Chappell, J., 1993. Holocene emergence and evolution of the McArthur River Delta, southwestern Gulf of Carpentaria, Australia. *Sedimentary Geology*, 83, 303-317.

Woodroffe, C. D, McLean, R., 1990. Microatolls and recent sea level change on coral atolls. *Nature*, 344, 531-534.

Woodroffe, C. D., Samosorn, B., Hua, Q., Hart, D. E. 2007. Incremental accretion of a sandy reef island over the past 3000 years indicated by component-specific radiocarbon dating. *Geophysics Research Letters* 34, L03602.

Woodroffe, S. A., Horton, B. P., 2005. Holocene sea-level changes in the Indo-Pacific. *Journal of Asian Earth Sciences* 25, 29-43.

Woodroffe, S. A., 2009. Testing models of mid to late Holocene sea-level change, north Queensland, Australia. *Quaternary Science Reviews* 28, 2474-2488.

Woodroffe, S. A., Horton, B. P., Larcombe, P., Whittaker, J. E., 2005. Intertidal mangrove foraminifera from the central Great Barrier Reef shelf, Australia, implications for sea-level reconstruction. *Journal of Foraminiferal Research* 35, 259-270.

Yokoyama, Y., Lambeck, L., De Deckker, P., Johnston, P., Fifield, L. K. 2000. Timing of the Last Glacial Maximum from observed sea-level minima. *Nature* 406, 713-716.

Yokoyama, Y., T.M. Esat, Lambeck, K. 2001a. Last glacial sea-level change deduced from uplifted coral terraces of Huon Peninsula, Papua New Guinea. *Quaternary International* 83-85:275-283.

Yokoyama, Y., A. Purcell, K. Lambeck, Johnston, P. 2001b. Shore-line reconstruction around Australia during the Last Glacial Maximum and Late Glacial Stage. *Quaternary International* 83-85:9-18.

Yu, K.F., Zhao, J.X., 2010. U-series dates of Great Barrier Reef corals suggest at least +0.7 m sea level ~7000 years ago. *The Holocene*, 20, 161-168.

Zhou, H., Zhao, J., Qing, W., Feng, Y., Tang, J., 2011. Speleothem-derived Asian summer monsoon variations in Central China, 54–46 ka. *Journal of Quaternary Science*, 26 (8), 781-790.